Title

mEAK-7 Forms an Alternative mTOR Complex with DNA-PKcs in Human Cancer

Authors

Nguyen, Joe Truong
Haidar, Fatima Sarah
Fox, Alexandra Lucienne
et al.

Publication Date

2019-07-01

DOI

10.1016/j.isci.2019.06.029

iScience

CellPress

Article

mEAK-7 Forms an Alternative mTOR Complex with DNA-PKcs in Human Cancer

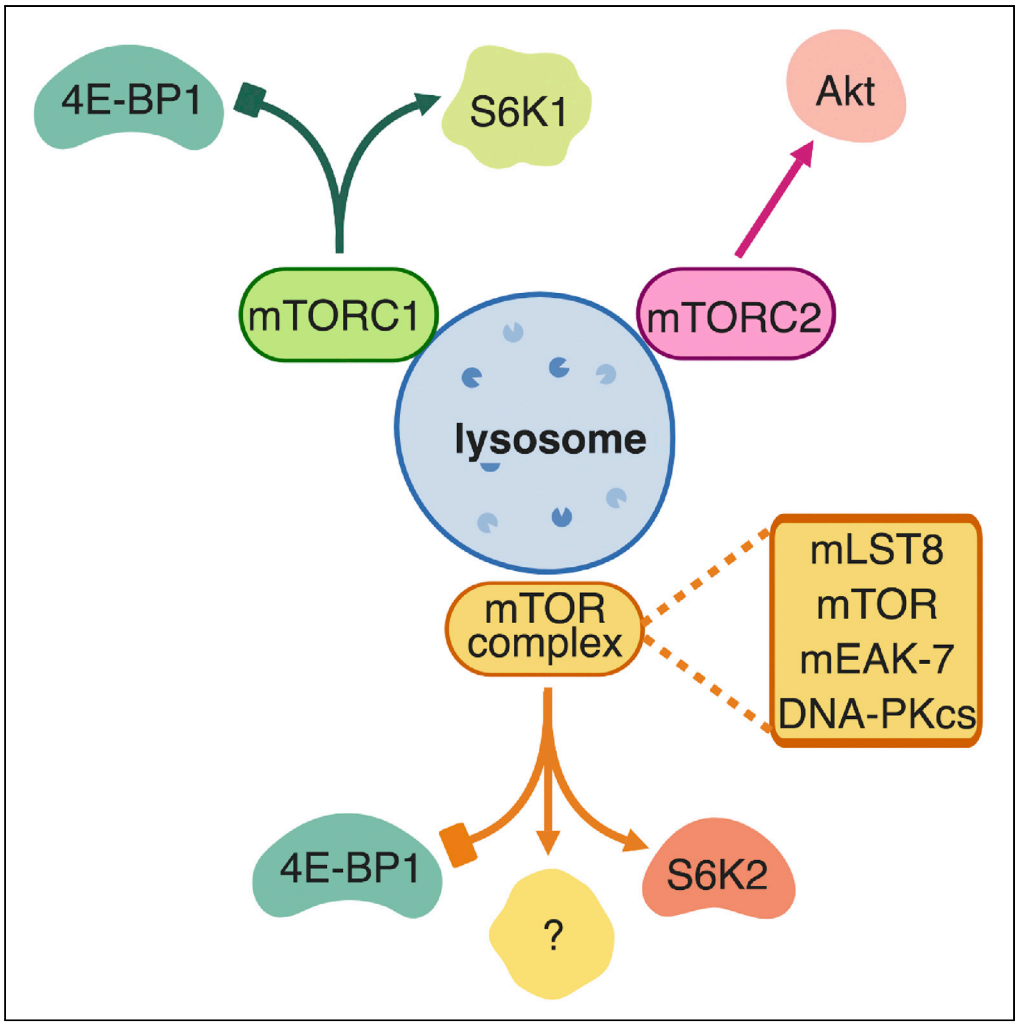

Joe Truong Nguyen, Fatima Sarah Haidar, Alexandra Lucienne Fox, Connor Ray, Daniela Baccelli Mendonça, Jin Koo Kim, Paul H. Krebsbach

pkrebsbach@dentistry.ucla.edu

HIGHLIGHTS

mEAK-7 forms an alternative mTOR complex with DNA-PK in human cancer

mEAK-7 is upregulated in the metastasized lymph nodes of patients with NSCLC

DNA-PK is essential for mEAK-7-mTOR-S6K2 signaling in human cancer

mEAK-7 is required for cancer cell clonogenicity and spheroid formation

Nguyen et al., iScience 17, 190–207
July 26, 2019
https://doi.org/10.1016/j.isci.2019.06.029

iScience

CellPress

Article

mEAK-7 Forms an Alternative mTOR Complex with DNA-PKcs in Human Cancer

Joe Truong Nguyen,[1,2] Fatima Sarah Haidar,[1,2] Alexandra Lucienne Fox,[1,2] Connor Ray,[1,2] Daniela Baccelli Mendonça,[1] Jin Koo Kim,[3] and Paul H. Krebsbach[3,4,*]

SUMMARY

MTOR associated protein, eak-7 homolog (mEAK-7), activates mechanistic target of rapamycin (mTOR) signaling in human cells through an alternative mTOR complex to regulate S6K2 and 4E-BP1. However, the role of mEAK-7 in human cancer has not yet been identified. We demonstrate that mEAK-7 and mTOR signaling are strongly elevated in tumor and metastatic lymph nodes of patients with non-small-cell lung carcinoma compared with those of patients with normal lung or lymph tissue. Cancer stem cells, CD44+/CD90+ cells, yield elevated mEAK-7 and activated mTOR signaling. mEAK-7 is required for clonogenic potential and spheroid formation. mEAK-7 associates with DNA-dependent protein kinase catalytic subunit isoform 1 (DNA-PKcs), and this interaction is increased in response to X-ray irradiation to regulate S6K2 signaling. DNA-PKcs pharmacologic inhibition or genetic knockout reduced S6K2, mEAK-7, and mTOR binding with DNA-PKcs, resulting in loss of S6K2 activity and mTOR signaling. Therefore, mEAK-7 forms an alternative mTOR complex with DNA-PKcs to regulate S6K2 in human cancer cells.

INTRODUCTION

Aberrant mechanistic target of rapamycin (mTOR) signaling has been observed in many types of human cancer (Saxton and Sabatini, 2017). Recently, mEAK-7 (mammalian EAK-7 or MTOR associated protein, eak-7 homolog) was identified as a molecular activator of mTOR signaling in human cells (Nguyen et al., 2018). Interestingly, mEAK-7 exhibits a preferential expression pattern in human cancer cell lines (Nguyen et al., 2018). Although EAK-7 regulates dauer formation and lifespan in *C. elegans* (Alam et al., 2010), the extent to which EAK-7 functions similarly in nematodes and mammals to regulate TOR/mTOR function is unknown.

mEAK-7 uses the S6K2/4E-BP1 axis to regulate mTOR signaling (Nguyen et al., 2018). S6K2 signaling has not been adequately delineated from that of S6K1 signaling owing to their assumed functional redundancies (Pardo and Seckl, 2013). However, in breast cancer cells, loss-of-function studies demonstrate that S6K1 and S6K2 have several different protein targets (Karlsson et al., 2015). In addition, canonical models of mTOR complex 1 (mTORC1), the traditional S6K regulators, and mTORC2 may not exist similarly in all cell types. As examples of this phenomena, an mTOR complex that involves GIT1, which is distinct from mTORC1 and mTORC2, has been identified in astrocytes (Smithson and Gutmann, 2016), and ETS Variant 7 is capable of binding to mTOR and sustaining mTOR signaling in the presence of rapamycin (Harwood et al., 2018). These pivotal findings disrupt conventional ideas regarding the existence of only two mTOR complexes and therefore suggest the possibility of other, unidentified mTOR complexes.

Although it is largely believed that mTOR signaling is suppressed under genotoxic stress via AMPK regulation of TSC2 (Feng et al., 2007), studies have demonstrated aberrant activation of mTOR signaling in response to DNA damage. For example, mTORC1 signaling inhibits DNA damage response mechanisms *in vitro* and *in vivo* through RNF168 (Xie et al., 2018). S6K2, another crucial mTOR target, may also function in the DNA damage response, as S6K2 knockdown results in strong reduction of mTOR signaling, even in the presence of DNA damage (Xie et al., 2018). Furthermore, CHK1 function relies on mTORC1 signaling in response to DNA damage repair processes. These findings suggest that mTOR signaling supports DNA damage responses (Zhou et al., 2017). In examining the role of radiation in DNA damage, sustained radiation treatment to mice activates mTOR signaling and oxidative stress in the intestine (Datta et al., 2014), whereas normal tissues undergoing long-term radiation stress exhibit activated mTOR signaling in mini pigs (Zhu et al., 2016). Thus, there is a rationale to treat patients with a combination of chemotherapeutics that induce DNA damage and mTOR inhibitors, like rapamycin, due to additive cytotoxic effects in breast

[1]Department of Biologic and Materials Sciences, University of Michigan, Ann Arbor, MI 48109, USA

[2]Biointerfaces Institute, University of Michigan, Ann Arbor, MI 48105, USA

[3]Section of Periodontics, School of Dentistry, University of California, Los Angeles, Los Angeles, CA 90095, USA

[4]Lead Contact

*Correspondence: pkrebsbach@dentistry.ucla.edu

https://doi.org/10.1016/j.isci.2019.06.029

carcinoma cell lines (Mondesire et al., 2004). These studies suggest that mTOR signaling and DNA damage repair processes may function synergistically in specific biologic contexts, such as during the downregulation of p53 via S6K-mediated activation of MDM2 (Lai et al., 2010), or the phosphorylation of 4E-BP1 phosphorylation in response to DNA damage (Braunstein et al., 2009). Thus, we posit a mechanism supporting sustained mTOR signaling after genotoxic stress, which may allow enhanced cancer cell survival through radiation resistance.

Cancer stem cells (CSCs) are known to be radiation resistant and thrive under genotoxic stress, but the molecular mechanisms responsible for these adaptations remain unknown (Bao et al., 2006; Diehn et al., 2009). CSCs are a self-renewing population of cells within a tumor mass (Al-Hajj et al., 2003), and mTOR signaling has been implicated in regulating pancreatic CSC viability and self-renewal (Matsubara et al., 2013). This suggests that this population of cancer cells utilizes mTOR signaling to contribute to the survival and pathogenicity of human cancers. Data from a medulloblastoma *in vivo* model of CSCs suggest that phosphatidylinositol 3-kinase (PI3K) signaling is activated in response to DNA damage, as indicated by S6 regulation, a crucial readout of mTOR signaling (Hambardzumyan et al., 2008). This substantive evidence suggests that mTOR signaling plays an important role in CSC DNA damage response and self-renewal.

Given that genotoxic stressors are capable of activating mTOR signaling, select CSCs were found to demonstrate radiation resistance, and because CSCs require mTOR signaling, we sought to determine the extent to which mEAK-7 contributes to radiation resistance and self-renewal in cancer cells through an alternative pathway involving mTOR.

RESULTS

mEAK-7 Protein Levels Are Elevated in Metastatic Human Non-Small Cell Lung Carcinoma Lymph Nodes

Although mEAK-7 protein levels appear to be disproportionately high in human cancer cell lines when compared with non-cancerous cells (Nguyen et al., 2018), this limited observation does not exclude the possibility that mEAK-7 is present in healthy human tissues, because mTOR expression is found in many tissue types (Kim et al., 2002). To gain a better understanding of the expression pattern of mEAK-7 in healthy human tissues, we accessed the GTEx database and identified basal-level expression of *MEAK7* in many human tissues (Figure 1A). The BioGPS database also confirmed that *MEAK7* is expressed in diverse tissue types (Figure S1A) (Wu et al., 2009, 2013, 2016). Thus, future analyses of mEAK-7 in healthy tissues are essential to understanding the role of mEAK-7 in mammalian development and metabolism.

To identify *MEAK7* genomic alterations in human patients with cancer, we accessed the cBioPortal database. Genetic modifications to *MEAK7* included deletions, copy number amplifications, and mutations; yet these modifications were found to be cancer type dependent (Figures 1B and 1C). For example, many prostate cancers exhibit *MEAK7* deletions, whereas breast cancers often sustain substantial *MEAK7* gene copy number amplification (Figure 1B). Because of these different genetic profiles, the search parameters were narrowed to include only gain of expression and copy number amplification. The percentage of patients that demonstrated either of these anomalies ranged between 5% and 50% (Figure 1C) (Cerami et al., 2012; Gao et al., 2013), demonstrating that *MEAK7* genetic modifications are cancer type specific and can be observed in a diverse array of human cancers.

The TCGA cBioPortal revealed high expression of *MEAK7* in patients with non-small-cell lung carcinoma (NSCLC) (Figure 1C). In addition, the majority of our first report into the mechanistic function of mEAK-7 was done in NSCLC lines, H1299 and H1975 (Nguyen et al., 2018). Therefore, the Oncomine database was accessed to analyze *MEAK7* expression patterns in lung carcinomas when compared with expression patterns in healthy lung tissue. Through two different lung cancer studies, *MEAK7* was found to be highly expressed in many NSCLCs and small cell lung carcinomas, when compared with normal lung tissue, suggesting that *MEAK7* may play a role in lung tumorigenesis (Figures 1D and 1E) (Rhodes et al., 2004). Also, an association was found between *MEAK7* expression and outcomes of patients with cancer. Patients who died from ductal breast carcinoma ($p = 2.72 \times 10^{-6}$, Fold Change: 2.136) and acute myeloid leukemia ($p = 7.99 \times 10^{-5,}$ Fold Change: 2.655) had enhanced *MEAK7* expression (Figures S1B and S1C) (Rhodes et al., 2004). Thus the *MEAK7* expression profile of patients with cancer may provide insight into predicting patient prognosis and survival.

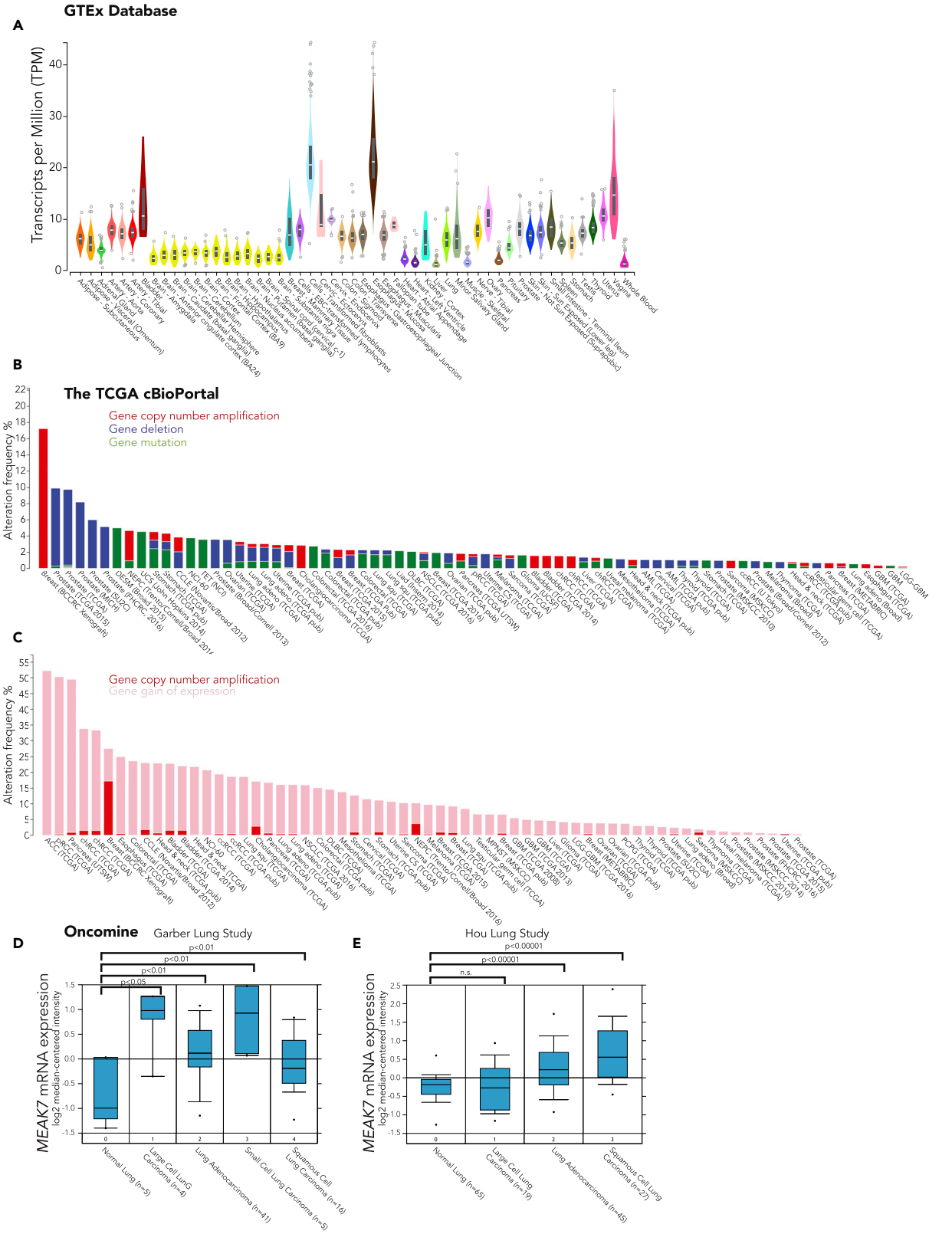
A
GTEx Database
Transcripts per Million (TPM)
B
The TCGA cBioPortal
Gene copy number amplification
Gene deletion
Gene mutation
Alteration frequency %
C
Gene copy number amplification
Gene gain of expression
Alteration frequency %
D
Oncomine
Garber Lung Study
MEAK7 mRNA expression
log2 median-centered intensity
Normal Lung (n=5)
Large Cell Lung Carcinoma (n=4)
Lung Adenocarcinoma (n=41)
Small Cell Lung Carcinoma (n=16)
Squamous Cell Lung Carcinoma (n=5)
E
Hou Lung Study
MEAK7 mRNA expression
log2 median-centered intensity
Normal Lung (n=65)
Large Cell Lung Carcinoma (n=19)
Lung Adenocarcinoma (n=45)
Squamous Cell Lung Carcinoma (n=27)

Figure 1. *MEAK7* Gene Expression Is Detected in Normal Human Cells and Upregulated in Select Human Cancer Types

(A) Genotype-Tissue Expression (GTEx) database analysis of *MEAK7* expression in normal human tissues.

(B and C) (B) The Cancer Genome Atlas cBioPortal analysis *MEAK7* for all genomic alterations or (C) for only gain of mRNA expression or amplification of gene copy number. The results shown are based on data generated by TCGA Research Network: http://cancergenome.nih.gov/.

(D and E) Oncomine analysis of *MEAK7* gene expression of patients with normal lung and lung cancer via two different studies: (D) Garber Lung Study analysis by Student's t test 2-sample equal variance and (E) Hou Lung Study analysis by Mann-Whitney U test, $p < 0.01$, 2-tailed.

In a screen of human squamous cell carcinomas, the UM-SCC-17A cell line (Brenner et al., 2010), derived from the primary laryngeal cancer site of a 48-year-old female patient, did not express detectable levels of mEAK-7 protein (Nguyen et al., 2018). Interestingly, the UM-SCC-17B cell line, derived from a metastatic site from the same patient, did express mEAK-7 (Nguyen et al., 2018). These findings suggest that increased expression of mEAK-7 may be associated with tumor metastasis. To test the hypothesis that elevated mEAK-7 protein levels are associated with cancer metastasis, the protein expression patterns of primary tumors and confirmed metastasizes closest to lymph tissues of patients with cancer were compared with healthy lung and lymph tissues. An NSCLC tissue microarray containing 30 individual pathologist-graded, patient-matched sections of primary tumors, as well as their normal adjacent tissue, and metastatic lymph nodes were stained and analyzed. mEAK-7 and ($Ser^{240/244}$) p-S6 protein levels were significantly elevated in the primary human tumor when compared with the normal adjacent tissue (Figures 2A–2C). Furthermore, mEAK-7 and ($Ser^{240/244}$) p-S6 protein levels were significantly greater in the metastatic lymph nodes when compared with both primary tumor and normal adjacent tissue (Figures 2A–2C). However, healthy adult lymph tissue did not yield substantial mEAK-7 or ($Ser^{240/244}$) p-S6 protein levels (Figure S2A). Thus, mEAK-7 protein and activated mTOR signaling was found to be enhanced in primary NSCLC, and substantially detected in metastasized lymph nodes, suggesting that mEAK-7 could function as a biomarker for patients with metastasized cancers.

As Oncomine databases demonstrate that higher *MEAK7* expression is associated with poor patient prognoses (Figures S1B and S1C), we sought to investigate this via a lung adenocarcinoma tissue microarray detailing patient survival data. The microarray stained with antibodies targeting endogenous mEAK-7 and ($Ser^{240/244}$) p-S6 and a Kaplan-Meier Survival Curve analysis illustrated that mEAK-7 protein levels were strongly associated with poor patient prognosis, specifically in patients with relapse following surgical intervention (Figure 2D).

Because mEAK-7 protein levels were highly expressed in metastasized lymph nodes, we tested the extent to which mEAK-7 is required for cell invasion *in vitro*. To test this, H1975 cells were treated with control or mEAK-7 small interfering RNA (siRNA) for 48 h and 50,000 cells were seeded into invasion chambers for 24 h. Results demonstrated a statistically significant reduction in cell invasion after 24 h (Figure 2E). Thus, mEAK-7 may be a clinically relevant biomarker for predicting the prognosis of patients with metastatic NSCLC.

Cancer Stem Cells Exhibit High Protein Levels of mEAK-7 and mTOR Signaling

mEAK-7 is a strong, positive regulator of mTOR signaling (Nguyen et al., 2018), and several groups have demonstrated that mTOR signaling is essential for CSC self-renewal (Matsubara et al., 2013) and radiation resistance (Fang et al., 2013). Therefore, we hypothesized that mEAK-7 is differentially expressed in the CSC versus non-CSC populations. Because the majority of information on human mEAK-7 has been demonstrated in NSCLC cell lines H1975 and H1299, we sought to determine the expression profile of mEAK-7 and mTOR signaling in NSCLC CSCs. These cells are best identified as being CD44+ (Leung et al., 2010) and CD90+ (Wang et al., 2013). Therefore, H1299 cells were subjected to fluorescence-activated cell sorting for the aforementioned markers. CD44+/CD90+ cells, representing 1% of all cells sorted, were analyzed for mEAK-7 and mTOR signaling (Figure 3A). Immunoblot analysis demonstrated that CD44+/CD90+ H1299 cells, when compared CD44−/CD90−, yielded greater protein levels of mEAK-7 and S6K2, as well as activated mTOR signaling, as measured via p-S6 and p-4E-BP1 protein levels (Figure 3B). The CD44+/CD90+ cell population expressed n-cadherin (Figure 3B), which is known as an essential component of the epithelial-mesenchymal transition state in CSCs and suggests that high levels of mEAK-7 in cancer cells are more likely to metastasize (Liu et al., 2014). Similar results were observed in CD44+/CD90+ H1975 cells (Figures S2B and S2C). Collectively, these results demonstrate that there is a selective expression profile of mEAK-7 and S6K2 in self-renewing CSCs.

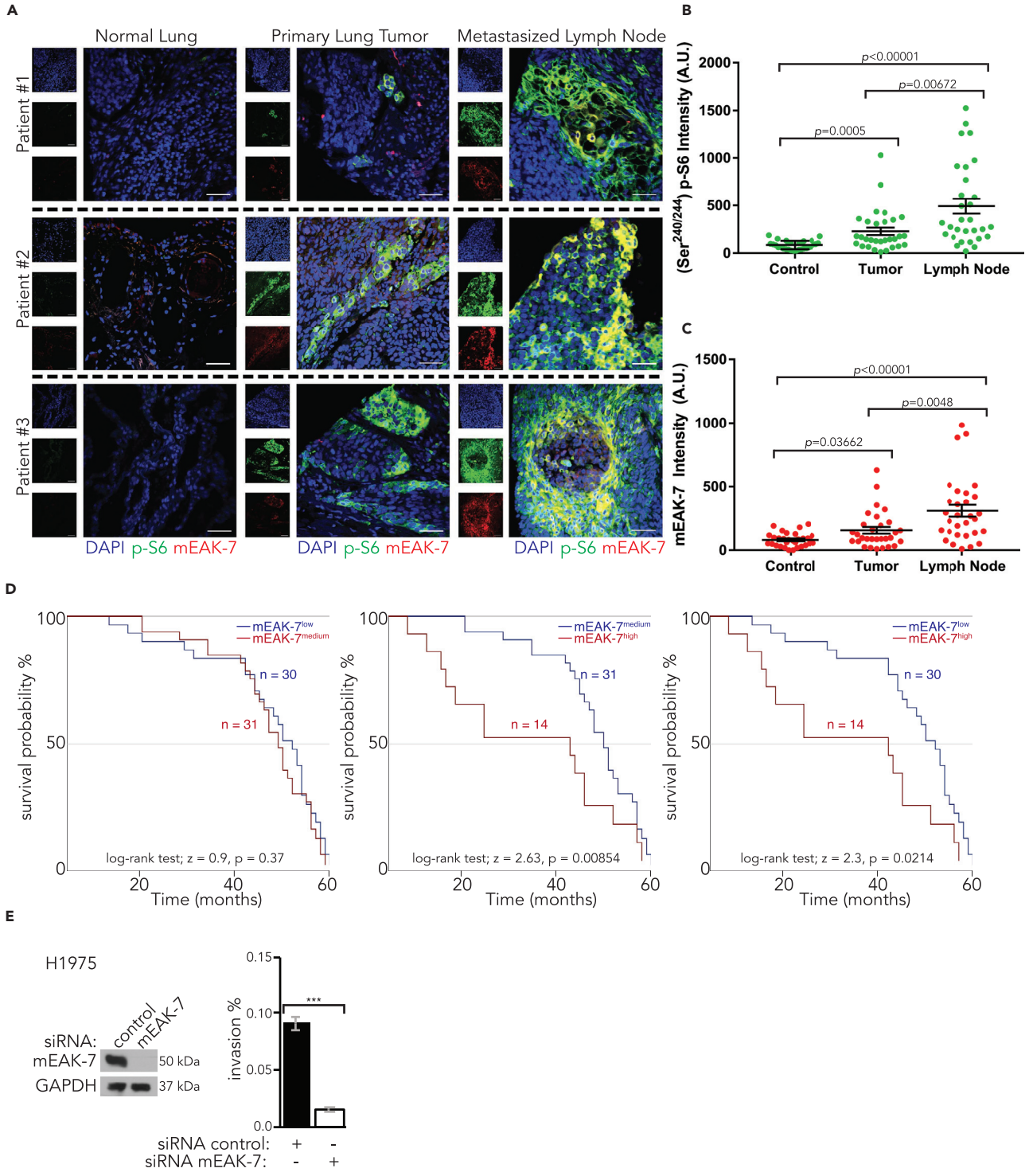

Figure 2. mEAK-7 Protein Levels Are High in Nearby Lymph Nodes of the Tumor Mass in Patients with NSCLC

(A) Three representative human patient tissue sections stained for (Ser$^{240/244}$) p-S6 and mEAK-7. Scale bar, 250 μm.

(B) Statistical analysis of 30 paired patients with NSCLC with the normal lung, primary tumor, and metastasized lymph node for (Ser$^{240/244}$) p-S6 staining. Mann-Whitney U test was used.

Figure 2. *Continued*

(C) Statistical analysis of 30 paired patients with NSCLC with the normal lung, primary tumor, and metastasized lymph node for mEAK-7 staining. Mann-Whitney U test was used.

(D) NSCLC tissue microarray analysis of Kaplan-Meier survival curves. Log rank test was used.

(E) H1975 cells were treated with control or mEAK-7 siRNA for 48 h; 50,000 cells were seeded into *in vitro* Matrigel-based invasion chambers and allowed to grow for 24 h. Analyzed by Student's t test (n = 6). ***$p < 0.0001$. Experiments were repeated at least six times.

mEAK-7 Is Necessary for Clonogenic Potential and Spheroid Formation in Human Cancer Cells

To test the hypothesis that mEAK-7 affects cell survival following X-ray irradiation damage, a 2D clonogenicity assay was used to assess the surviving fraction of irradiated cancer cells (Franken et al., 2006; Puck and Marcus, 1956). H1299 and H1975 cells were treated with control or mEAK-7 siRNA for 48 h and then subjected to no treatment or X-ray irradiation of 2 or 6 Gy. These cells were then reseeded into new 60-mm tissue culture plates and allowed to grow for 10 days. In both H1299 and H1975 cells, clonogenic potential was significantly decreased after mEAK-7 knockdown, but little additional effects were found after exposure to 2- and 6-Gy X-ray irradiation in both H1299 and H1975 cells (Figures 3C–3H). This suggests that mEAK-7 alone is capable of regulating clonogenic potential to a dramatic extent. In H1299 and H1975 cells, similar results were observed at higher cell seeding densities (Figure S2D) or by utilizing a different siRNA mEAK-7 (Figures S3A and S3B), demonstrating that mEAK-7 enhances the clonogenic potential of human cancer cells in response to DNA damage.

Two-dimensional assays measuring clonogenic potential demonstrate the essential role of mEAK-7 in the DNA damage response, whereas 3D assays better simulate *in vivo* conditions. The spheroid-forming assay is a widely accepted experimental strategy to identify stem cell self-renewal in mammalian cell systems *in vitro* and *in vivo* (Pastrana et al., 2011). Furthermore, CSCs are the principal cancer cell population responsible for spheroid formation (Weiswald et al., 2015). Thus, to test the effect of mEAK-7 on spheroid size and formation, H1975 cells were treated with control or mEAK-7 siRNA for 48 h, subjected to no treatment or 2- or 6-Gy X-ray irradiation, and subsequently seeded in ultra-low attachment dishes for 1 week. mEAK-7 knockdown resulted in a dramatic reduction in spheroid size with no treatment, or 2- or 6-Gy treatment (Figure 4A). In addition, the gross number of spheroids formed was significantly reduced after mEAK-7 knockdown, and even further reduced following 2- or 6-Gy X-ray irradiation treatment (Figure 4B). Similar results were observed when H1975 cells were seeded at a lower density (Figure S3C) and when a different mEAK-7 siRNA was used in both H1299 and H1975 cells (Figures S3D and S3E). These results collectively indicate that mEAK-7 plays a significant role in cancer cell spheroid formation.

mEAK-7 Is Necessary for Chemoresistance, Radiation Resistance, and Sustained DNA Damage-Mediated mTOR Signaling in Human Cancer Cells

Although X-ray irradiation is a potent inducer of the DNA damage response pathway, we hypothesized that other forms of genotoxic stress may similarly regulate mEAK-7. Cisplatin is a chemotherapeutic drug often used to treat patients with cancer with solid tumors. Cisplatin is widely used for the treatment of solid tumors because it has the ability to activate the DNA damage response and allow cells to undergo apoptosis. Although the mechanism of action would take 20 years to unravel, it was clear that cisplatin produced DNA adducts and forced double-stranded breaks in the DNA. However, following initial tumor regression, a fraction of solid tumors become chemoresistant (Galluzzi et al., 2012). mTOR signaling can be activated during cisplatin treatment of ovarian cancer cells over time, as measured by enhanced (Thr^{389}) p-S6K1 protein levels (Peng et al., 2010). As mEAK-7 is required for mTOR signaling, we tested the hypothesis that mEAK-7 is an essential modulator of mTOR signaling following genotoxic stress induced by cisplatin treatment. To test the extent to which genotoxic stress modifies mEAK-7 activity, H1299 cells were treated with mEAK-7 siRNA for 48 h. Next, these cells were treated with either DMSO or 10 μM cisplatin for 4 or 8 h. mEAK-7 protein levels were increased in response to DNA damage by cisplatin treatment. Furthermore, mEAK-7 was required for regulation of (Ser^{65}) p-4E-BP1, an indicator of mTOR signaling (Figure 4C). Therefore, cisplatin is capable of regulating mEAK-7-mediated mTOR signaling.

mEAK-7 Knockdown Impairs the DNA Damage Response and Enhances Noxa Levels after X-Ray Irradiation

Cancer cells utilize many mechanisms to promote radioresistance in response to cancer therapies (Kim et al., 2009). To determine the role of X-ray irradiation on mEAK-7 and the DNA damage response,

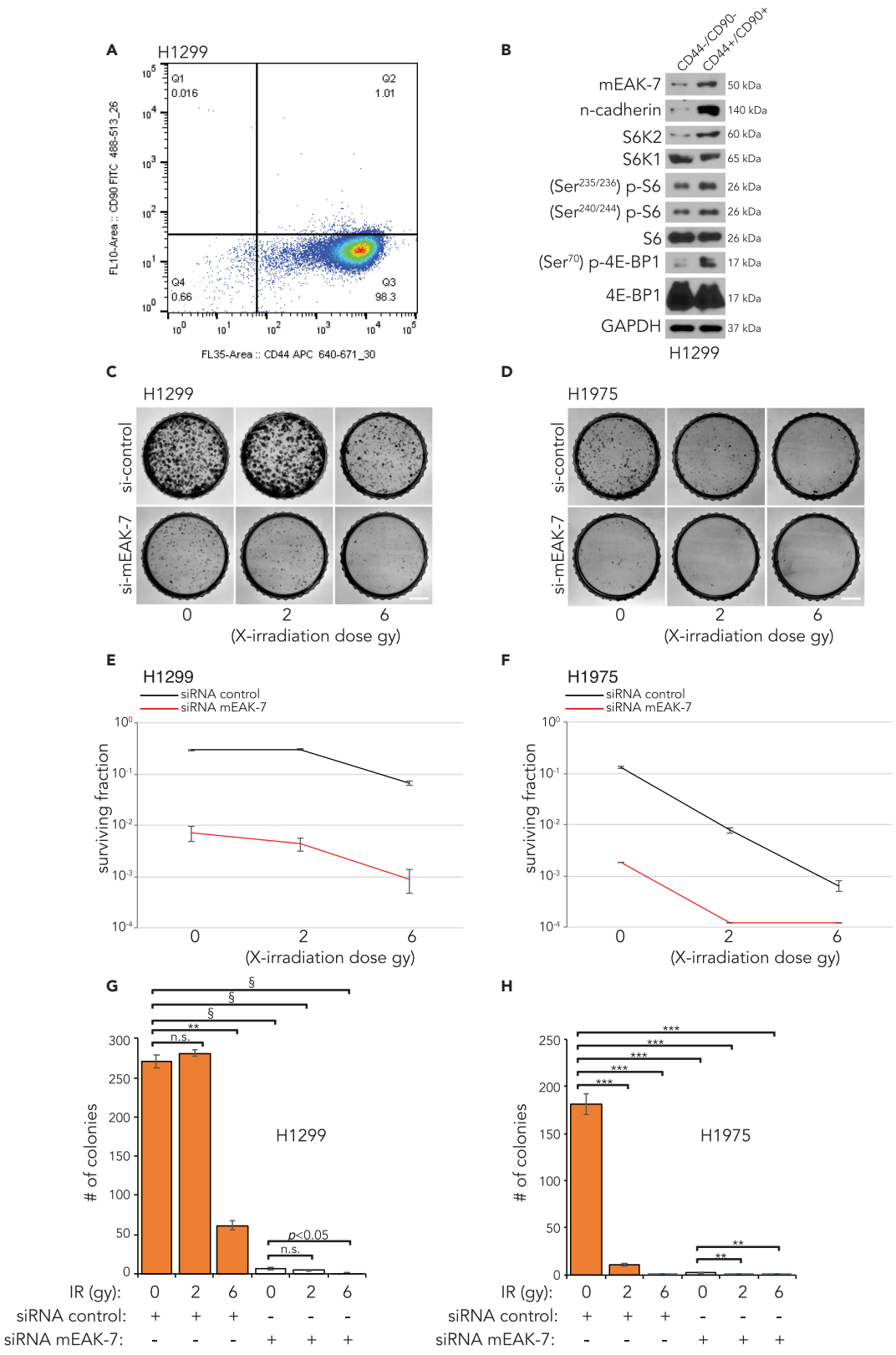
A
H1299
Q1
0.016
Q2
1.01
Q4
0.66
Q3
98.3
FL10-Area :: CD90 FITC 488-513_26
FL35-Area :: CD44 APC 640-671_30
B
CD44-/CD90-
CD44+/CD90+
mEAK-7
n-cadherin
S6K2
S6K1
(Ser235/236) p-S6
(Ser240/244) p-S6
S6
(Ser70) p-4E-BP1
4E-BP1
GAPDH
50 kDa
140 kDa
60 kDa
65 kDa
26 kDa
26 kDa
26 kDa
17 kDa
17 kDa
37 kDa
H1299
C
H1299
si-control
si-mEAK-7
0
2
6
(X-irradiation dose gy)
D
H1975
si-control
si-mEAK-7
0
2
6
(X-irradiation dose gy)
E
H1299
siRNA control
siRNA mEAK-7
surviving fraction
(X-irradiation dose gy)
F
H1975
siRNA control
siRNA mEAK-7
surviving fraction
(X-irradiation dose gy)
G
H1299
# of colonies
n.s.
**
§
p<0.05
IR (gy): 0 2 6 0 2 6
siRNA control: + + + - - -
siRNA mEAK-7: - - - + + +
H
H1975
# of colonies
***
**
IR (gy): 0 2 6 0 2 6
siRNA control: + + + - - -
siRNA mEAK-7: - - - + + +

Figure 3. mEAK-7 Is Expressed in CD44+/CD90+ Group and Required for Clonogenic Potential and Radiation Resistance

(A) Flow sort diagram depicting the CD44+/CD90+ cell population in H1299 cells.

(B) Immunoblot analysis of CD44−/CD90− and CD44+/CD90+ H1299 cells for mEAK-7 and mTOR signaling.

(C) H1299 cells were treated with control or mEAK-7 siRNA for 48 h, X-ray irradiated at 2 or 6 Gy, and 2,500 cells were seeded into 60-mm tissue culture plates (TCPs) and grown for 10 days.

(D) H1975 cells were treated with control or mEAK-7 siRNA for 48 h and subjected to no treatment or 2- and 6-Gy X-ray irradiation, and 5,000 cells were seeded into 60-mm TCPs and grown for 10 days. Scale bars, 2.5 mm.

(E) H1299 surviving fraction analysis for (C).

(F) H1975 surviving fraction analysis for (D).

(G) H1299 colony number graphs for (C).

(H) H1975 colony number graphs for (D).

Analysis of clonogenic assay via Student's t test. $^{**}p < 0.001$, $^{***}p < 0.0001$, $^{§}p < 0.000001$. All experiments were repeated at least three times, and (C–H) was repeated six times.

H1975 cells were treated with control or mEAK-7 siRNA, and X-ray irradiated with 20 Gy for up to 2 h. H1975 cells treated with mEAK-7 siRNA exhibited a dramatic increase in Noxa levels (Figure 4D). We also found similar results in H1299 cells treated with mEAK-7 siRNA and subjected to X-ray irradiation (Figure S3F). Upregulation of Noxa occurs in response to DNA damage after mEAK-7 knockdown (Figure 4D), which ultimately leads to cellular apoptosis (Ploner et al., 2008), suggesting that mEAK-7 plays a role in the DNA damage response and cancer cell survival. Noxa is known to be regulated by p53-dependent mechanisms through oncogene-independent apoptosis induced by genotoxic stressors, where p53 activates both survival and apoptotic pathways through p21WAF1/Cip1 (Shibue et al., 2003). However, Noxa has also been shown to function through p53-independent mechanisms, where ATF3 and ATF4 are induced by cisplatin, a DNA-damaging agent, and downregulation of ATF3 or ATF4 reduces Noxa expression because ATF3 and ATF4 bind to and cooperatively activate the Noxa promoter (Sharma et al., 2018). As H1975 is a p53 wild-type NSCLC line and H1299 is a p53-null NSCLC line, mEAK-7 may regulate Noxa expression through a p53-independent mechanism.

The comet assay is used to quantify intracellular DNA damage resulting from an insufficient DNA damage repair response in eukaryotic cells (Collins, 2004). H1299 and H1975 cells were independently embedded in an agarose gel and lysed, thereby releasing intracellular DNA. During gel electrophoresis, DNA fragments migrate toward the anode, resulting in a "comet" pattern with a trail of DNA fragments, such that a longer trail signifies more fragments, and therefore more DNA damage (Ostling and Johanson, 1984). Owing to the dramatic results from radiation treatment with mEAK-7 knockdown in the clonogenicity (Figures 3C–3H) and spheroid assays (Figures 4A and 4B), we hypothesized that mEAK-7 plays a crucial role in the DNA damage repair pathways. The visualization of DNA strand migration via the comet assay, and subsequent quantification of that migration, allowed us to predict the relative levels of the DNA repair response. H1299 and H1975 cells were treated with control or mEAK-7 siRNA and subjected to no treatment or 2- or 6-Gy X-ray irradiation for 30 min. Comet pattern formations, quantified as tail DNA %, were enhanced in H1299 and H1975 cells treated with mEAK-7 siRNA and X-ray irradiation (Figures 4E–4H), suggesting mEAK-7 is necessary for the DNA repair response in these cancer cells.

mEAK-7 Interacts with DNA-PKcs in Response to X-Ray Irradiation Damage

To determine the extent to which mEAK-7 regulates genotoxic activation of mTOR signaling, we sought to identify interacting partners of mEAK-7 by transducing H1299 cells with a lentivirus expressing pLenti-GIII-HA(c-term)mEAK-7. Through hemagglutinin (HA)-mEAK-7 immunoprecipitation (IP) and mass spectrometric (MS) analysis, a list of proteins that potentially interact with mEAK-7 was generated (Table S1). DNA-dependent protein kinase catalytic subunit isoform 1 (DNA-PKcs) scored the highest with 241 exclusive spectral counts and 36% protein coverage (Figure 5A). As with the canonical role of DNA-PKcs in the DNA damage response, ataxia mutated (ATM) and ataxia telangiectasia- and Rad3-related (ATR) also play essential and redundant roles in repairing damaged DNA, because all three share similar targets in response to DNA damage (Ciccia and Elledge, 2010; Nguyen et al., 2018). These data suggest that other phosphatidylinositol 3-kinase-related kinase (PIKK) members, like DNA-PKcs and mTOR, could also work in concert to regulate metabolism. Thus, we posited that mEAK-7 regulates mTOR signaling, in part, through the interaction with DNA-PKcs.

To confirm our IP/MS results, protein lysates were harvested from H1299 cells stably transduced with HA-mEAK-7. Exogenous mEAK-7 interacted with endogenous DNA-PKcs (Figures 5B and 5C). Under UV B

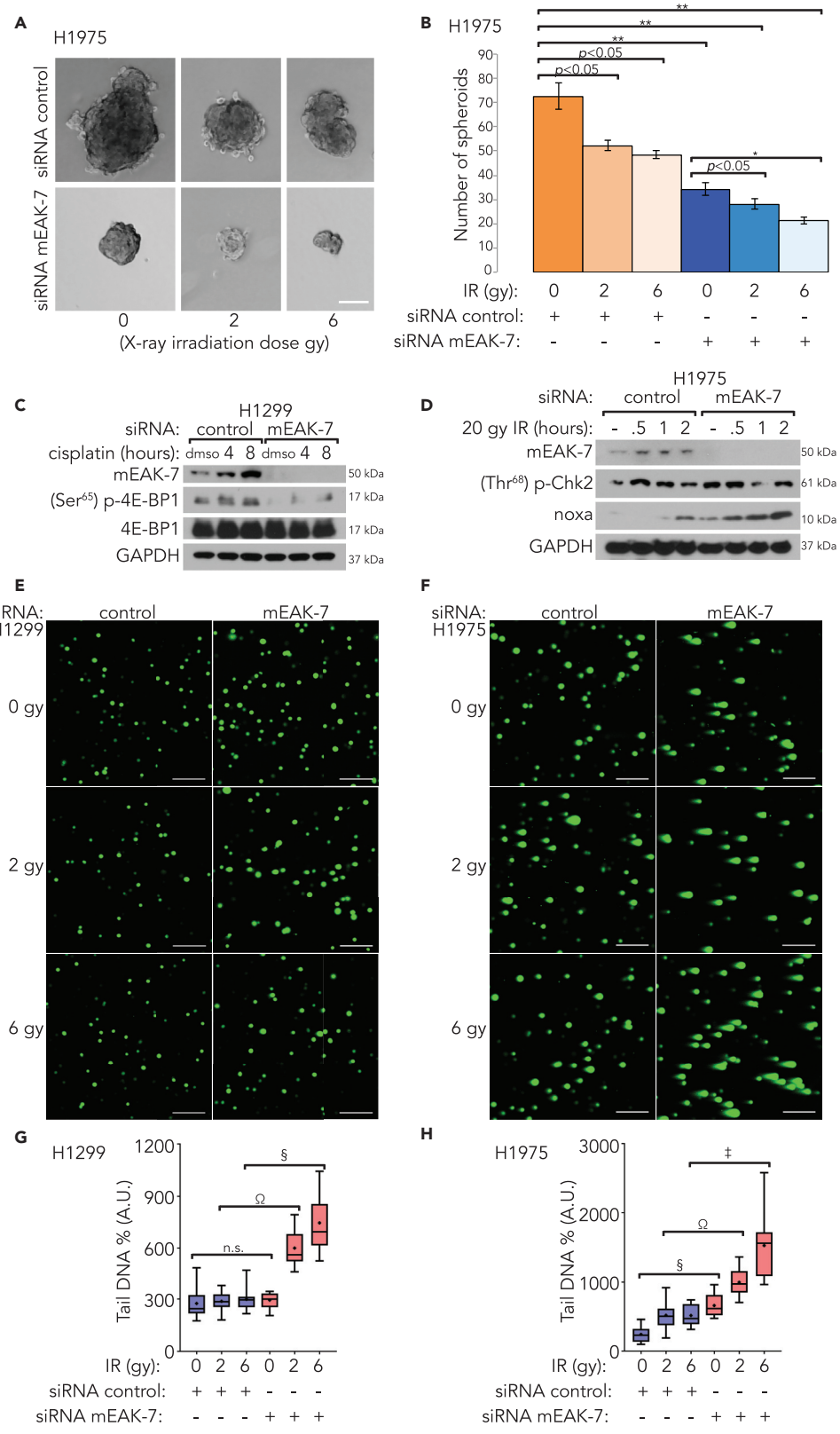
A
H1975
siRNA control
siRNA mEAK-7
0
2
6
(X-ray irradiation dose gy)
B
H1975
Number of spheroids
p<0.05
p<0.05
**
**
**
*
p<0.05
IR (gy): 0 2 6 0 2 6
siRNA control: + + + - - -
siRNA mEAK-7: - - - + + +
C
H1299
siRNA: control mEAK-7
cisplatin (hours): dmso 4 8 dmso 4 8
mEAK-7
(Ser65) p-4E-BP1
4E-BP1
GAPDH
50 kDa
17 kDa
17 kDa
37 kDa
D
H1975
siRNA: control mEAK-7
20 gy IR (hours): - .5 1 2 - .5 1 2
mEAK-7
(Thr68) p-Chk2
noxa
GAPDH
50 kDa
61 kDa
10 kDa
37 kDa
E
siRNA: control mEAK-7
H1299
0 gy
2 gy
6 gy
F
siRNA: control mEAK-7
H1975
0 gy
2 gy
6 gy
G
H1299
Tail DNA % (A.U.)
n.s.
Ω
§
IR (gy): 0 2 6 0 2 6
siRNA control: + + + - - -
siRNA mEAK-7: - - - + + +
H
H1975
Tail DNA % (A.U.)
§
Ω
‡
IR (gy): 0 2 6 0 2 6
siRNA control: + + + - - -
siRNA mEAK-7: - - - + + +

Figure 4. mEAK-7 Is Required for Spheroid Formation and Is Necessary for an Effective DNA Damage Response

(A) Images of spheroids. H1975 cells were treated with control or mEAK-7 siRNA, X-ray irradiated at 2 or 6 Gy, and 10,000 cells were seeded into 60-mm ultra-low attachment plates and grown for 10 days. Scale bar, 125 μm.

(B) Quantification of spheroid formation and analysis via Student's t test (n = 6) of (A). *$p < 0.01$, **$p < 0.001$.

(C) H1299 cells were treated with control or mEAK-7 siRNA and with DMSO or 10 μM cisplatin for 4 or 8 h, and mTOR signaling was analyzed.

(D) H1975 cells were treated with control or mEAK-7 siRNA and X-ray irradiated at 20 Gy for 30 min, 1 h, or 2 h and analyzed for Noxa expression by DNA damage response.

(E and F) H1299 and H1975 cells were treated with control or mEAK-7 siRNA and X-ray irradiated at 2 or 6 Gy for 30 min and assessed via the comet assay to detect damaged DNA. Scale bar, 250 μm.

(G and H) Statistical analysis via Student's t test (n = 15) of (E and F) represented as box plots. *$p < 0.01$, **$p < 0.001$, $^{\ddagger}p < 0.00001$, $^{\S}p < 0.000001$, $^{\Omega}p<0.0000001$. All experiments were repeated at least three times.

irradiation, DNA-PKcs has been shown to interact with mTOR kinase and SIN1 to affect mTORC2 signaling in epithelial skin keratinocytes, but the molecular rationale for this interaction remains elusive (Tu et al., 2013). Furthermore, nuclear DNA-PKcs transverses to the cytosol in response to DNA damage (Tu et al., 2013). This ability to travel to the cytoplasm, combined with evidence that DNA-PKcs can activate metabolism-related genes, suggests a role for DNA-PKcs in metabolic signaling.

Because mEAK-7 interacts with mTOR in increasing amounts of amino acid, insulin, or nutrient conditions (Nguyen et al., 2018), we sought to determine the extent to which mEAK-7 increases its binding to DNA-PKcs after DNA damage. H1299 cells stably expressing HA-mEAK-7 were subjected to no treatment or X-ray irradiated with 10 Gy for 30 or 60 min, and results revealed that mEAK-7 increasingly interacted with DNA-PKcs over time in response to DNA damage (Figure 5D). These data suggest that mEAK-7 associates with DNA-PKcs and mTOR to form a third mTOR complex (mTORC3), distinct from mTORC1 and mTORC2.

First, to determine the extent to which S6K2 is required for mTOR signaling following X-ray irradiation, H1975 and H1299 cells were treated with controls or two unique S6K1 or S6K2 siRNAs. Results revealed that p-S6 levels were abrogated after S6K2 knockdown in H1975 and H1299 cells (Figures S4A and S4B), suggesting that S6K2 is necessary for sustained S6 phosphorylation in response to DNA damage. S6K2 is capable of binding to mTOR in the presence of nutrient stimulation (Nguyen et al., 2018), but it is unknown whether S6K2 binds to DNA-PKcs. As mEAK-7 is required for the mTOR-S6K2 axis (Nguyen et al., 2018), DNA-PKcs and S6K2 binding was tested to determine the extent to which mEAK-7 and DNA-PKcs form a complex that regulates mTOR signaling through S6K2. To test whether S6K2 interacts with DNA-PKcs in the presence of DNA damage, H1299 cells were transiently transfected with pcDNA3-HA-S6K2-WT; subsequently, they were X-ray irradiated with 10 Gy for 1 h and HA-S6K2 was immunoprecipitated. X-ray irradiation considerably increased the interaction between DNA-PKcs and HA-S6K2, whereas it had little to no influence on mTOR and HA-S6K2 interaction (Figure 5E). Conversely, HA-S6K1 binding to DNA-PKcs was observed, but there was a severe reduction in binding after DNA damage, suggesting that S6K1 is not the main downstream target of DNA-PKcs after DNA damage (Figure S4C). These findings were reproduced under nutrient stimulation as well, where DNA-PKcs enhances binding to HA-S6K2 and DNA-PKcs diminishes binding to HA-S6K1 (Figure S4D). DNA-PKcs is capable of interacting with S6K2 to regulate its function in response to DNA damage. To determine if mTOR is required for mEAK-7-mediated DNA-PKcs function and interaction, mTOR was knocked down with two different mTOR siRNAs, which resulted in a dramatic reduction of DNA-PKcs interaction with endogenous mEAK-7 (Figure 5F). This collective evidence links mEAK-7 to the major metabolic sensor, mTOR, and the crucial DNA damage repair regulator, DNA-PKcs.

Although we previously established the function of mEAK-7 in mTOR signaling under nutrient conditions (Nguyen et al., 2018), its role in mTOR signaling under genotoxic stressors remains unknown. To test the hypothesis that mEAK-7 is required for mTOR activation after DNA damage, H1299 and H1975 cells were treated with control or mEAK-7 siRNA for 48 h in DMEM with 10% fetal bovine serum (FBS). Two different conditions were compared: 1-h nutrient starvation with 30-min nutrient replenishment was compared with 10-Gy X-irradiation for 30 min. Under these conditions, mEAK-7 was also capable of regulating sustained activation of mTOR signaling after X-ray irradiation in NSCLC (Figure 5G). Thus, mEAK-7 is capable of regulating nutrient-dependent mTOR signaling, as well as X-ray irradiated activation of mTOR signaling.

A

#	Identified human proteins	M.W. (kDa)	% coverage	# counts
1	DNA-dependent protein kinase catalytic subunit isoform	1469	36.10	241
2	filamin-A isoform 1	280	51.90	164
3	60 kDa heat shock protein, mitochondrial	61	66.70	113
4	fatty acid synthase	273	30.00	101
5	filamin-C isoform a	291	32.00	83
6	glyceraldehyde-3-phosphate dehydrogenase	36	68.10	70
7	keratin 1	66	46.30	66
8	dynein, cytoplasmic, heavy chain 1, isoform CRA_b	525	15.80	59
9	general transcription factor II-I isoform 1	112	43.30	55
10	vimentin	54	57.30	40

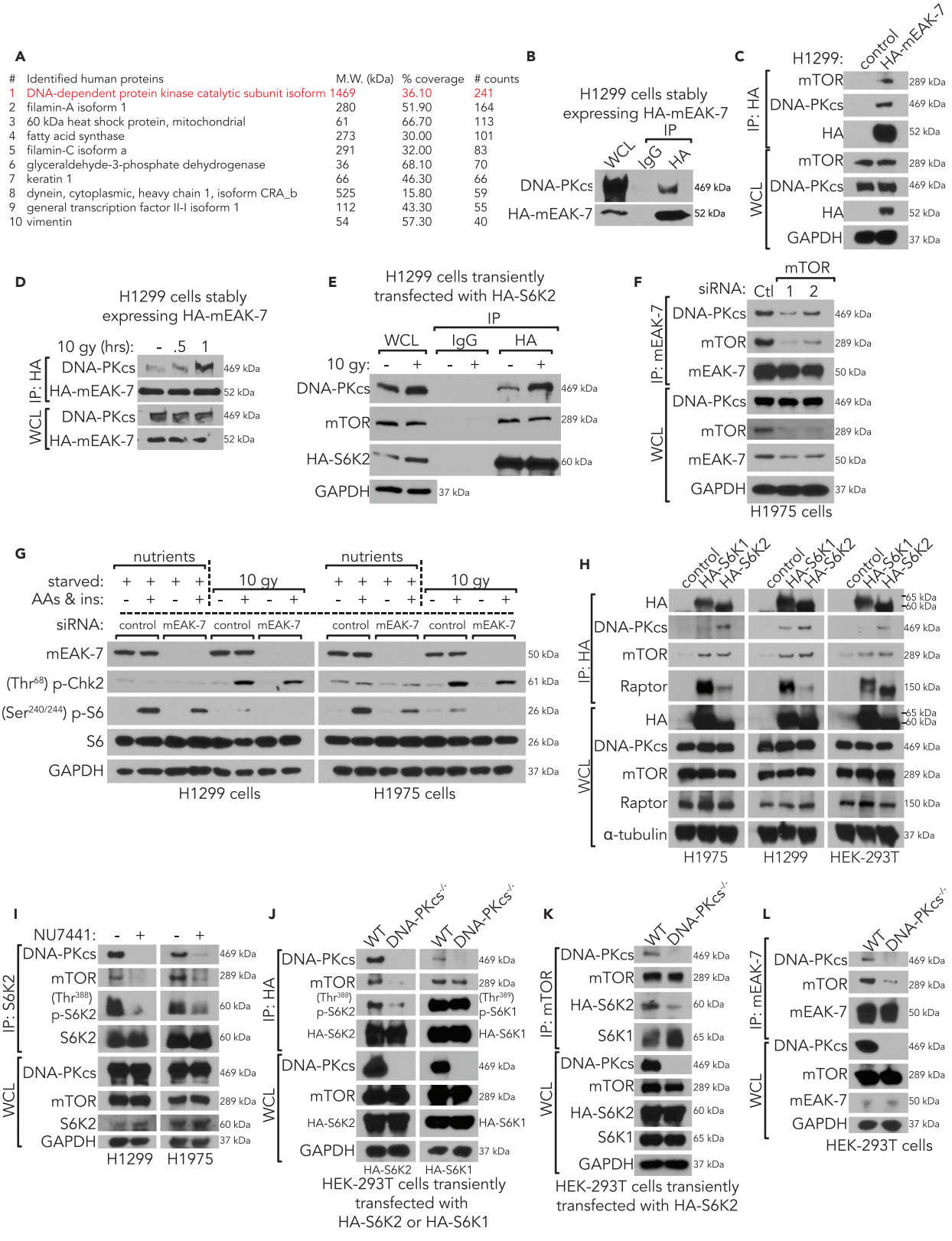

Figure 5. mEAK-7 Forms a Third mTOR Complex with DNA-PKcs to Regulate S6K2 Activity

(A) H1299 cells stably expressing HA-mEAK-7 were lysed in 3-((3-cholamidopropyl) dimethylammonio)-1-propanesulfonate (CHAPS) buffer, HA-mEAK-7 was immunoprecipitated, and co-immunoprecipitated proteins were analyzed for mass spectrometry quantitative profiling.

(B) H1299 cells stably expressing HA-mEAK-7 were lysed in NP40 lysis buffer and using IgG control antibody or HA-tag antibody, HA-mEAK-7 was immunoprecipitated to check DNA-PKcs interaction.

(C) Non-transduced H1299 cells or H1299 cells stably expressing HA-mEAK-7 were lysed in CHAPS lysis buffer, and HA-tag antibody was used for immunoprecipitation to check DNA-PKcs or mTOR interaction.

(D) H1299 cells stably expressing HA-mEAK-7 were untreated or X-ray irradiated at 10 Gy for 30 min and 1 h and lysed in NP40 lysis buffer. HA-mEAK-7 was immunoprecipitated to check DNA-PKcs interaction.

(E) H1299 cells were transiently transfected with pcDNA3-HA-S6K2 and then untreated or X-ray irradiated at 10 Gy for 1 h. HA-S6K2 was immunoprecipitated to check DNA-PKcs or mTOR interaction.

(F) H1975 cells were transiently transfected with control or mTOR #1 or mTOR #2 siRNA for 48 h. Cells were collected in CHAPS, and endogenous mEAK-7 was immunoprecipitated to check DNA-PKcs interaction.

(G) H1299 and H1975 cells were transiently transfected with control or mEAK-7 siRNA for 48 h. Cells were subsequently starved of nutrients for 1 h and replenished with $DMEM^{+AAs}$ and 10 μM insulin for 30 min or cultured normally and treated with 10-Gy X-ray irradiation for 30 min. Immunoblot analysis was conducted for mTOR signaling proteins.

(H) H1975, H1299, and HEK293T cells were transfected with no plasmid, pRK7-HA-S6K1-WT, and pcDNA3-HA-S6K2. HA-tag antibody was immunoprecipitated and probed for DNA-PKcs, mTOR, and Raptor.

(I) H1299 and H1975 cells were treated with either DMSO or NU7441 (DNA-PKcs inhibitor) at 5 μM for 2 h and mixed in fresh DMEM with 10% FBS. Cells were collected in CHAPS, S6K2 was immunoprecipitated, and immunoblots were utilized to assess mTOR signaling. GAPDH was used for loading controls.

(J) $DNA\text{-}PKcs^{WT}$ and $DNA\text{-}PKcs^{-/-}$ HEK293T cells were transfected with pcDNA3-HA-S6K2 or pRK7-HA-S6K1-WT. Before protein isolation, cells were fed fresh DMEM with 10% FBS for 1 h before collection in CHAPS. HA-tag antibody was immunoprecipitated and probed for mTOR and activated S6K2 signaling.

(K) Experimental protocols were repeated from (J), and mTOR antibody was immunoprecipitated and probed for mTOR, HA-S6K2, and S6K1.

(L) $DNA\text{-}PKcs^{WT}$ and $DNA\text{-}PKcs^{-/-}$ HEK-293T cells were collected in CHAPS lysis buffer. Endogenous mEAK-7 was immunoprecipitated and probed for mTOR and DNA-PKcs. All experiments were repeated at least three times.

Next, to determine the relative binding affinities of S6K1 and S6K2 to their most relevant complex, we transfected H1299, H1975, and HEK-293T cells with HA-S6K1 or HA-S6K2 and immunoprecipitated HA-S6K1 or HA-S6K2 to probe for mTOR, raptor, and DNA-PKcs binding. Interestingly, we discovered that HA-S6K1 is capable of binding to DNA-PKcs, but HA-S6K2 binds to DNA-PKcs to a significantly larger extent (Figure 5H). Furthermore, we found that raptor binding to HA-S6K1 was strong, whereas HA-S6K2 binding to raptor was weaker (Figure 5H). This suggests that S6K1 and S6K2 have preferential binding affinities to mTORC1, or alternative mTOR complexes. Finally, to test the extent to which DNA-PKcs activity is required for S6K2 function, H1299 and H1975 cells were treated with either DMSO or 5 μM NU7441, a highly specific chemical inhibitor of DNA-PKcs, for 2 h under freshly stimulated 10% FBS medium. NU7441 is 1,000× more specific for DNA-PKcs than PI3K and 200× more specific for DNA-PKcs than mTOR. DNA-PKcs inhibition resulted in a substantial decrease in S6K2/mTOR/DNA-PKcs binding, as well as S6K2 functional activity (Figure 5I). These results suggest that mEAK-7 structurally links DNA-PKcs and S6K2 to mTOR signaling.

Although pharmacologic agents are potent molecules to dissect the downstream pathways within cells, they still may yield non-specific targeting. To rule out non-specific interactions of DNA-PKcs inhibitors with other kinases, we obtained validated $DNA\text{-}PKcs^{-/-}$ HEK293T cells (Neal et al., 2016). In $DNA\text{-}PKcs^{-/-}$ cells, IP demonstrated that HA-S6K2 phosphorylation was diminished and HA-S6K2 binding to mTOR was reduced, but HA-S6K1 phosphorylation and HA-S6K1 binding to mTOR were minimally affected (Figure 5J). IP of mTOR in $DNA\text{-}PKcs^{-/-}$ cells transfected with HA-S6K2 resulted in abrogated binding to HA-S6K2 and increased binding to HA-S6K1, demonstrating that mTOR utilizes DNA-PKcs to form a new complex to target S6K2 (Figure 5K). Finally, loss of DNA-PKcs inhibited the ability of mEAK-7 to bind to mTOR, suggesting that mEAK-7, DNA-PKcs, and mTOR form a stable complex to regulate S6K2 (Figure 5L).

mEAK-7 Is Required for Sustained IR-Mediated mTOR Signaling in Human Cancer Cells and Loss of mEAK-7 Results in Enhanced PARP Cleavage

As we determined that mEAK-7 knockdown combined with X-ray irradiation resulted in strong Noxa upregulation, we posited that other markers of cell apoptosis would also be affected by mEAK-7. PARP cleavage has been shown to be an essential mediator of cell apoptosis and cell death (Morales et al., 2014). To determine the extent to which mEAK-7 regulates PARP cleavage, H1299 cells treated with mEAK-7 siRNA resulted in enhanced levels of cleaved PARP (Figure 6A). These results suggest mEAK-7 is required for radiation resistance and that the loss of mEAK-7 results in severe reduction of mTOR signaling and enhanced PARP cleavage.

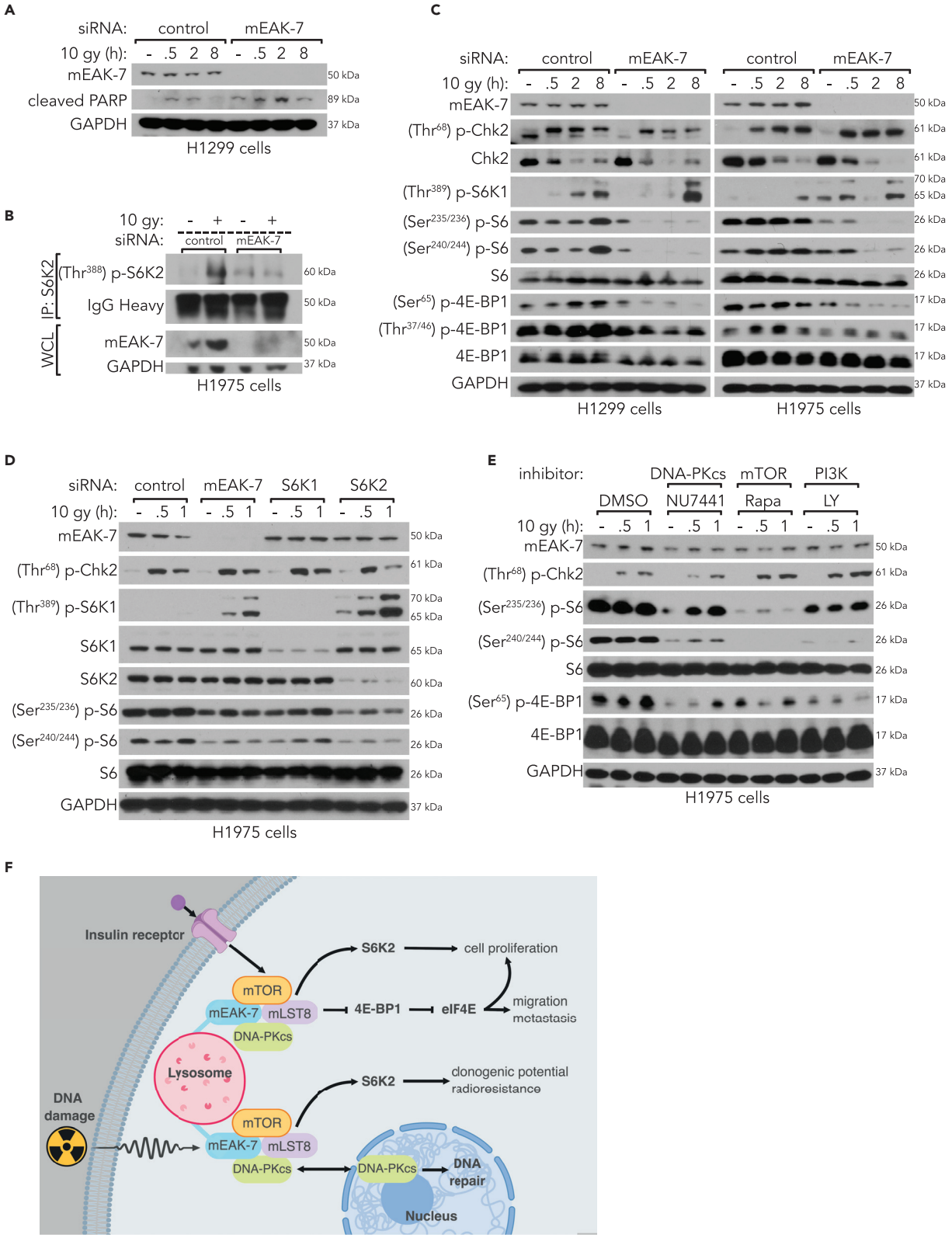
A
siRNA: control mEAK-7
10 gy (h): - .5 2 8 - .5 2 8
mEAK-7
cleaved PARP
GAPDH
50 kDa
89 kDa
37 kDa
H1299 cells
B
10 gy: - + - +
siRNA: control mEAK-7
IP: S6K2
WCL
(Thr388) p-S6K2
IgG Heavy
mEAK-7
GAPDH
60 kDa
50 kDa
50 kDa
37 kDa
H1975 cells
C
siRNA: control mEAK-7 control mEAK-7
10 gy (h): - .5 2 8 - .5 2 8 - .5 2 8 - .5 2 8
mEAK-7
(Thr68) p-Chk2
Chk2
(Thr389) p-S6K1
(Ser235/236) p-S6
(Ser240/244) p-S6
S6
(Ser65) p-4E-BP1
(Thr37/46) p-4E-BP1
4E-BP1
GAPDH
50 kDa
61 kDa
61 kDa
70 kDa
65 kDa
26 kDa
26 kDa
26 kDa
17 kDa
17 kDa
17 kDa
37 kDa
H1299 cells
H1975 cells
D
siRNA: control mEAK-7 S6K1 S6K2
10 gy (h): - .5 1 - .5 1 - .5 1 - .5 1
mEAK-7
(Thr68) p-Chk2
(Thr389) p-S6K1
S6K1
S6K2
(Ser235/236) p-S6
(Ser240/244) p-S6
S6
GAPDH
50 kDa
61 kDa
70 kDa
65 kDa
65 kDa
60 kDa
26 kDa
26 kDa
26 kDa
37 kDa
H1975 cells
E
inhibitor: DMSO DNA-PKcs NU7441 mTOR Rapa PI3K LY
10 gy (h): - .5 1 - .5 1 - .5 1 - .5 1
mEAK-7
(Thr68) p-Chk2
(Ser235/236) p-S6
(Ser240/244) p-S6
S6
(Ser65) p-4E-BP1
4E-BP1
GAPDH
50 kDa
61 kDa
26 kDa
26 kDa
26 kDa
17 kDa
17 kDa
37 kDa
H1975 cells
F
Insulin receptor
mTOR
mEAK-7
mLST8
DNA-PKcs
S6K2
cell proliferation
4E-BP1
eIF4E
migration
metastasis
Lysosome
DNA damage
S6K2
clonogenic potential
radioresistance
mTOR
mEAK-7
mLST8
DNA-PKcs
DNA-PKcs
DNA repair
Nucleus

Figure 6. mEAK-7 and DNA-PKcs Are Required for X-Ray Irradiation-Mediated mTOR Signaling

(A) H1299 cells were treated with control or mEAK-7 siRNA for 48 h; X-ray irradiated at 10 Gy for 30 min, 2 h, and 8 h; and analyzed for PARP cleavage.

(B) H1975 cells were transiently transfected with control or mEAK-7 siRNA for 48 h. Next, cells were treated with 10-Gy X-ray irradiation for 30 min, followed by IP of endogenous S6K2, and probed for activated S6K2 signaling.

(C) H1299 and H1975 cells were treated with control or mEAK-7 siRNA for 48 h; X-ray irradiated at 10 Gy for 30 min, 2 h, and 8 h; and analyzed for mTOR signaling.

(D) H1975 cells were treated with control, mEAK-7, S6K1, and S6K2 siRNA for 48 h; X-ray irradiated at 10 Gy for 30 min and 1 h; and analyzed for mTOR signaling.

(E) H1975 cells were treated with DMSO, DNA-PKcs inhibitor (5 μM NU7441 IC50 = 14 nM), mTOR inhibitor (100 nM rapamycin, IC50 = 1 nM), and PI3K inhibitor (50 μM LY249002, IC50 = 2.3 μM) for 1 h before being treated with X-ray irradiation at 10 Gy for 30 min and 1 h and analyzed for mTOR signaling.

(F) Working model for a mEAK-7-mTOR-DNA-PKcs complex. All experiments were repeated at least three times. GAPDH was used for loading controls.

Next, we posited that mEAK-7 was required for S6K2 phosphorylation and activation after X-ray irradiation. H1975 cells were treated with control or mEAK-7 siRNA for 48 h and 10-Gy X-ray irradiation for 30 min. IP of endogenous S6K2 demonstrated that mEAK-7 knockdown resulted in a dramatic decrease in X-ray irradiation-mediated S6K2 phosphorylation (Figure 6B). Use of a different mEAK-7 siRNA also resulted in a decrease in S6K2 phosphorylation after DNA damage (Figure S4E). Moreover, the literature details examples of sustained mTOR signaling following DNA damage as a modulator of self-renewal and radiation resistance (Silvera et al., 2017). To test the hypothesis that mEAK-7 is necessary for sustained X-ray irradiation-mediated mTOR signaling, H1299 and H1975 cells were treated with control or mEAK-7 siRNA for 48 h in DMEM with 10% FBS and then with 10-Gy X-irradiation for 30 min, 2 h, or 8 h. H1299 and H1975 cells treated with mEAK-7 siRNA exhibited abrogated mTOR signaling over time (Figure 6C). These results were also confirmed in MDA-MB-231 cells, a triple-negative breast carcinoma cell line (Figure S5). Therefore, these results suggest that mEAK-7 is required for sustained mTOR signaling as well as cell survival after DNA damage, and that the loss of mEAK-7 results in severe reduction of mTOR signaling and enhanced PARP cleavage.

Both S6K1 and S6K2 are essential components of mTOR signaling that are described to have similar, but distinct, cellular roles in human development and disease (Pardo and Seckl, 2013). To elucidate the roles of S6K1 and S6K2 following X-ray irradiation damage, ($Ser^{240/244}$) p-S6 levels were measured in response to siRNA-mediated knockdown of mEAK-7, S6K1, or S6K2 and treatment with 10-Gy X-ray irradiation. H1975 cells were treated with control, mEAK-7, S6K1, or S6K2 siRNA for 48 h in DMEM with 10% FBS. Subsequently, the cells were treated with 10-Gy X-ray irradiation for 30 min or 1 h. mEAK-7 and S6K2 knockdown each markedly reduced ($Ser^{240/244}$) p-S6 levels, but S6K1 knockdown did not have a substantial effect on ($Ser^{240/244}$) p-S6 levels (Figure 6D). These results mirrored the nutrient conditions, as previously published (Nguyen et al., 2018). Furthermore, mEAK-7 or S6K2 knockdown dramatically increased (Thr^{389}) p-S6K1 levels following X-ray irradiation-induced damage, suggesting a specific role for S6K2 and mEAK-7 during X-ray irradiation-mediated mTOR signaling (Figure 6D).

Although some reports suggest a possible intersection of DNA-PKcs and mTOR signaling, these ideas have not yet been fully validated across a spectrum of cell types and experimental conditions. In an effort to test the hypothesis that DNA-PKcs and mTOR signaling depend on mEAK-7 to carry out a shared function, we treated H1299 and H1975 cells with NU7441. NU7441 treatment significantly reduced infrared (IR)-mediated mTOR signaling in a dose-dependent manner, but had little effect on (Ser^{2448}) p-mTOR levels (Figure S6A). To determine whether NU7441 significantly inhibits IR-induced activation of mTOR signaling compared with other mTOR inhibitors, we used specific inhibitors of DNA-PKcs (NU7441), mTOR (rapamycin), and PI3K (LY249002). Inhibition of DNA-PKcs, mTOR, or PI3K significantly decreased mTOR signaling in H1975 cells (Figure 6E). These results were also consistent in H1299 cells (Figure S6B). In conclusion, DNA-PKcs is a fundamental component of a novel mTOR complex that regulates the mEAK-7/mTOR signaling axis and targets S6K2.

DISCUSSION

Surgical intervention and radiation therapy are common treatment modalities for patients with solid tumors. However, in many patients the condition relapses as tumors acquire resistance through intratumoral evolution (McGranahan and Swanton, 2017). CD44+/CD90+ cells have been identified as a unique population of cancer cells that may be required for the regulation of chemo- and radioresistance through PI3K and mTOR signaling (Chang et al., 2013). Furthermore, the literature demonstrates that S6K2 inhibits apoptosis in lung cancer (Pardo et al., 2006) and that S6K2 amplification is associated with more aggressive

forms of breast cancer (Pérez-Tenorio et al., 2011). Similarly, a retrospective study conducted on patients with breast cancer demonstrated that 4E-BP1 and S6K2 were correlated with poor prognosis and endocrine resistance (Karlsson et al., 2013). This evidence, combined with our findings that mTOR signaling, mEAK-7, and S6K2 are upregulated in CD44+/CD90+ cancer cell populations, suggests that mEAK-7 is involved in mTOR signaling in CSCs.

Although CD44+/CD90+ cells demonstrate radiation resistance and self-renewal capacity that correlate with elevated mEAK-7 protein levels, loss of mEAK-7 alone does not result in enhanced cell apoptosis in human cancer cells (Nguyen et al., 2018). The combination of DNA damage and loss of mEAK-7 is capable of enhancing cell apoptosis. This is likely because the mechanisms that support cell survival and self-renewal are different. As PI3K and mTOR signaling are crucial regulators of radiation resistance and self-renewal in many carcinomas, including cervical carcinoma (Kim et al., 2010), head and neck squamous cell carcinoma (Leiker et al., 2015), and breast carcinoma (Steelman et al., 2011), it is important to note that mEAK-7 is also a strong effector of these processes. Specifically, CSCs have been identified as a cell population that modulates radiation resistance and self-renewal in solid tumors (Pajonk et al., 2010).

Alternative mTOR signaling appears to be upregulated in human patients with cancer, specifically in patients with metastatic disease (Figures 2A–2C). Here, DNA-PKcs was identified as a new interacting partner of mEAK-7 (Figures 5A–5H) and may participate in the regulation of this alternative mTOR signaling. DNA-PKcs is a member of the PIKK family that includes mTOR, ATM, ATR, suppressor of morphogenesis in genitalia (SMG1), and transformation/transcription domain-associated protein (TRRAP) (Lovejoy and Cortez, 2009). DNA-PKcs has been extensively studied in the context of non-homologous end joining and homologous recombination, both of which are DNA damage repair pathways (Smith and Jackson, 1999). PIKKs typically have redundant cellular roles, depending on their cellular localization and biologic context. For example, DNA-PKcs, ATM, and ATR all have similar cellular targets in response to DNA damage (Ciccia and Elledge, 2010). Intriguingly, DNA-PKcs was found to play a critical role in metabolic gene regulation in response to insulin (Wong et al., 2009). However, DNA-PKcs predominantly resides in the nucleus, so it was initially unclear how DNA-PKcs could exit the nucleus to affect nutrient metabolism. The literature supports the observation that pockets of DNA-PKcs exists in lipid rafts outside of the nucleus, suggesting the existence of a different role for DNA-PKcs in cytoplasmic cellular signaling (Lucero et al., 2003). In support of these diverse findings, we demonstrate that DNA-PKcs interacts with mEAK-7 to regulate mTOR signaling, predominantly through S6K2.

In mini pigs, mTOR signaling is enhanced in salivary glands 5 days after treatment with X-ray irradiation (Zhu et al., 2016). In addition, PI3K and mTOR are essential regulators of radiation resistance in prostate cancer cells (Chang et al., 2014) as dual PI3K-mTOR inhibitors re-sensitize cancer cells to radiation treatment (Mukherjee et al., 2012). Here, we demonstrate that mEAK-7 is required for the sustained activity of mTOR signaling following X-ray irradiation damage. Continued investigation of mEAK-7 and other molecular machinery that regulates IR damage-mediated activation of mTOR signaling will allow for the creation of targeted inhibitors promoting radiation re-sensitization.

As the role of mEAK-7 is further studied in the context of human disease, its unique role in nutrient-sensing and DNA damage response (Figure 6F) will likely expand. S6K2 is a crucial component of mTOR signaling that has been overlooked (Pardo and Seckl, 2013). Yet, many studies demonstrate that S6K2 is associated with human diseases, including non-small-cell lung cancer (Pardo et al., 2006) and late-stage breast cancer (Karlsson et al., 2015). We determined that there are high mEAK-7 protein levels in the tumors and lymph nodes of patients with metastatic cancer, that mEAK-7^{high} patients have poor prognoses, and that mEAK-7 is essential for self-renewal and radioresistance. To determine the evolutionary benefit that cancer cells gain from upregulating mEAK-7, future research should be focused on elucidating the mechanisms allowing tumorigenesis in a broader range of cancers. Likewise, development of mEAK-7 inhibitors may benefit patients with metastatic cancers that demonstrate aberrant mTOR signaling associated with high levels of mEAK-7.

Limitations of the Study

Here, we report that DNA-PKcs is a binding partner of the mEAK-7-mTOR complex. Some pitfalls of these studies are that we lack animal models that could recapitulate human disease. As most of our work is to identify novel binding partners and the detailed mechanism by which they interact, future studies will be

required to examine the role of mEAK-7 *in vivo*. Also, our inhibitor studies against DNA-PKcs, although severalfold more specific to DNA-PKcs versus mTOR, could yield some off-target effects and DNA-PKcs knockout cell lines may not recapitulate all of physiology, suggesting that genetic approaches *in vivo* are required to understand the role of DNA-PKcs binding to mTOR to form mTORC3. Thus the role of this alternative complex to canonical mTOR signaling requires further study in animal models where mTOR signaling is required for eukaryotic development and disease progression.

METHODS

All methods can be found in the accompanying Transparent Methods supplemental file.

SUPPLEMENTAL INFORMATION

Supplemental Information can be found online at https://doi.org/10.1016/j.isci.2019.06.029.

ACKNOWLEDGMENTS

We thank M. Wicha for expertise and use of equipment. We thank F.S.H. and H. Amatullah for replicating key experiments. We thank Dr. Kathryn Meek from Michigan State University for the use of the HEK-293T DNA-PK$^{-/-}$, clone 7. The Genotype-Tissue Expression (GTEx) Project was supported by the Common Fund of the Office of the Director of the National Institutes of Health, and by NCI, NHGRI, NHLBI, NIDA, NIMH, and NINDS. The data used for the analyses described in this manuscript were obtained from the GTEx Portal on 04/08/18 using term "*MEAK7*". Figure 6F was "Created with BioRender." We thank our funding sources: National Institute of Dental and Craniofacial Research (1F30DE026048–01, R01-DE016530, and T32-DE007057) and Stuart & Barbara Padnos Research Award from the Comprehensive Cancer Center at the University of Michigan.

AUTHOR CONTRIBUTIONS

J.T.N, F.S.H., A.L.F., C.R., D.B.M., J.K.K., and P.H.K. designed experiments and analyzed results. J.T.N., F.S.H., A.L.F., and C.R. carried out experiments. J.T.N. and P.H.K. are responsible for the major ideas. J.T.N. and P.H.K. wrote the paper. J.T.N., F.S.H., C.R., D.B.M., A.L.F., J.K.K., and P.H.K. edited the manuscript.

DECLARATIONS OF INTERESTS

The authors declare no competing interests.

Received: December 5, 2018
Revised: April 30, 2019
Accepted: June 19, 2019
Published: July 26, 2019

REFERENCES

Al-Hajj, M., Wicha, M.S., Benito-Hernandez, A., Morrison, S.J., and Clarke, M.F. (2003). Prospective identification of tumorigenic breast cancer cells. Proc. Natl. Acad. Sci. U S A *100*, 3983–3988.

Alam, H., Williams, T.W., Dumas, K.J., Guo, C., Yoshina, S., Mitani, S., and Hu, P.J. (2010). EAK-7 controls development and life span by regulating nuclear DAF-16/FoxO activity. Cell Metab. *12*, 30–41.

Bao, S., Wu, Q., McLendon, R.E., Hao, Y., Shi, Q., Hjelmeland, A.B., Dewhirst, M.W., Bigner, D.D., and Rich, J.N. (2006). Glioma stem cells promote radioresistance by preferential activation of the DNA damage response. Nature *444*, 756–760.

Braunstein, S., Badura, M.L., Xi, Q., Formenti, S.C., and Schneider, R.J. (2009). Regulation of protein synthesis by ionizing radiation. Mol. Cell. Biol. *29*, 5645–5656.

Brenner, J.C., Graham, M.P., Kumar, B., Saunders, L.M., Kupfer, R., Lyons, R.H., Bradford, C.R., and Carey, T.E. (2010). Genotyping of 73 UM-SCC head and neck squamous cell carcinoma cell lines. Head Neck *32*, 417–426.

Cerami, E., Gao, J., Dogrusoz, U., Gross, B.E., Sumer, S.O., Aksoy, B.A., Jacobsen, A., Byrne, C.J., Heuer, M.L., Larsson, E., et al. (2012). The cBio cancer genomics portal: an open platform for exploring multidimensional cancer genomics data. Cancer Discov. *2*, 401–404.

Chang, L., Graham, P.H., Hao, J., Ni, J., Bucci, J., Cozzi, P.J., Kearsley, J.H., and Li, Y. (2013). Acquisition of epithelial-mesenchymal transition and cancer stem cell phenotypes is associated with activation of the PI3K/Akt/mTOR pathway in prostate cancer radioresistance. Cell Death Dis. *4*, e875.

Chang, L., Graham, P.H., Hao, J., Ni, J., Bucci, J., Cozzi, P.J., Kearsley, J.H., and Li, Y. (2014). PI3K/Akt/mTOR pathway inhibitors enhance radiosensitivity in radioresistant prostate cancer cells through inducing apoptosis, reducing autophagy, suppressing NHEJ and HR repair pathways. Cell Death Dis. *5*, e1437.

Ciccia, A., and Elledge, S.J. (2010). The DNA damage response: making it safe to play with knives. Mol. Cell *40*, 179–204.

Collins, A.R. (2004). The comet assay for DNA damage and repair: principles, applications, and limitations. Mol. Biotechnol. *26*, 249–261.

Datta, K., Suman, S., and Fornace, A.J., Jr. (2014). Radiation persistently promoted oxidative stress,

activated mTOR via PI3K/Akt, and downregulated autophagy pathway in mouse intestine. Int. J. Biochem. Cell Biol. *57*, 167–176.

Diehn, M., Cho, R.W., Lobo, N.A., Kalisky, T., Dorie, M.J., Kulp, A.N., Qian, D., Lam, J.S., Ailles, L.E., Wong, M., et al. (2009). Association of reactive oxygen species levels and radioresistance in cancer stem cells. Nature *458*, 780–783.

Fang, D.D., Zhang, C.C., Gu, Y., Jani, J.P., Cao, J., Tsaparikos, K., Yuan, J., Thiel, M., Jackson-Fisher, A., Zong, Q., et al. (2013). Antitumor efficacy of the dual PI3K/mTOR inhibitor PF-04691502 in a human xenograft tumor model derived from colorectal cancer stem cells harboring a PIK3CA mutation. PLoS One *8*, e67258.

Feng, Z., Hu, W., de Stanchina, E., Teresky, A.K., Jin, S., Lowe, S., and Levine, A.J. (2007). The regulation of AMPK beta1, TSC2, and PTEN expression by p53: stress, cell and tissue specificity, and the role of these gene products in modulating the IGF-1-AKT-mTOR pathways. Cancer Res. *67*, 3043–3053.

Franken, N.A., Rodermond, H.M., Stap, J., Haveman, J., and van Bree, C. (2006). Clonogenic assay of cells in vitro. Nat. Protoc. *1*, 2315–2319.

Galluzzi, L., Senovilla, L., Vitale, I., Michels, J., Martins, I., Kepp, O., Castedo, M., and Kroemer, G. (2012). Molecular mechanisms of cisplatin resistance. Oncogene *31*, 1869–1883.

Gao, J., Aksoy, B.A., Ugur Dogrusoz, G.D., Gross, B., Sumer, S.O., Sun, Y., Jacobsen, A., Sinha, R., Larsson, E., Cerami, E., et al. (2013). Integrative analysis of complex cancer genomics and clinical profiles using the cBioPortal. Sci. Signal. *6*, pl1.

Hambardzumyan, D., Becher, O.J., Rosenblum, M.K., Pandolfi, P.P., Manova-Todorova, K., and Holland, E.C. (2008). PI3K pathway regulates survival of cancer stem cells residing in the perivascular niche following radiation in medulloblastoma in vivo. Genes Dev. *22*, 436–448.

Harwood, F.C., Geltink, R.I.K., O'Hara, B.P., Cardone, M., Janke, L., Finkelstein, D., Entin, I., Paul, L., Houghton, P.J., and Grosveld, G.C. (2018). ETV7 is an essential component of a rapamycin-insensitive mTOR complex in cancer. Sci. Adv. *4*, 1–18.

Karlsson, E., Magic, I., Bostner, J., Dyrager, C., Lysholm, F., Hallbeck, A.L., Stal, O., and Lundstrom, P. (2015). Revealing different roles of the mTOR-targets S6K1 and S6K2 in breast cancer by expression profiling and structural analysis. PLoS One *10*, e0145013.

Karlsson, E., Pérez-Tenorio, G., Amin, R., Bostner, J., Skoog, L., Fornander, T., Sgroi, D.C., Nordenskjöld, B., Hallbeck, A.-L., and Stål, O. (2013). The mTOR effectors 4EBP1 and S6K2 are frequently coexpressed, and associated with a poor prognosis and endocrine resistance in breast cancer- a retrospective study including patients from the randomised Stockholm tamoxifen trials. Breast Cancer Res. *15*, 1–12.

Kim, D.-H., Sarbassov, D.D., Al, S.M., King, J.E., Latek, R.R., Erdjument-Bromage, H., Tempst, P., and Sabatini, D.M. (2002). mTOR interacts with raptor to form a nutrient-sensitive complex that signals to the cell growth machinery. Cell *110*, 163–175.

Kim, M.K., Kim, T.J., Sung, C.O., Choi, C.H., Lee, J.W., Kim, B.G., and Bae, D.S. (2010). High expression of mTOR is associated with radiation resistance in cervical cancer. J. Gynecol. Oncol. *21*, 181–185.

Kim, Y., Joo, K.M., Jin, J., and Nam, D.-H. (2009). Cancer stem cells and their mechanism of chemo-radiation resistance. Int. J. Stem Cells *2*, 109–114.

Lai, K.P., Leong, W.F., Chau, J.F., Jia, D., Zeng, L., Liu, H., He, L., Hao, A., Zhang, H., Meek, D., et al. (2010). S6K1 is a multifaceted regulator of Mdm2 that connects nutrient status and DNA damage response. EMBO J. *29*, 2994–3006.

Leiker, A.J., DeGraff, W., Choudhuri, R., Sowers, A.L., Thetford, A., Cook, J.A., Van Waes, C., and Mitchell, J.B. (2015). Radiation enhancement of head and neck squamous cell carcinoma by the dual PI3K/mTOR inhibitor PF-05212384. Clin. Cancer Res. *21*, 2792–2801.

Leung, E.L., Fiscus, R.R., Tung, J.W., Tin, V.P., Cheng, L.C., Sihoe, A.D., Fink, L.M., Ma, Y., and Wong, M.P. (2010). Non-small cell lung cancer cells expressing CD44 are enriched for stem cell-like properties. PLoS One *5*, e14062.

Liu, S., Cong, Y., Wang, D., Sun, Y., Deng, L., Liu, Y., Martin-Trevino, R., Shang, L., McDermott, S.P., Landis, M.D., et al. (2014). Breast cancer stem cells transition between epithelial and mesenchymal states reflective of their normal counterparts. Stem Cell Reports *2*, 78–91.

Lovejoy, C.A., and Cortez, D. (2009). Common mechanisms of PIKK regulation. DNA Repair (Amst) *8*, 1004–1008.

Lucero, H., Gae, D., and Taccioli, G.E. (2003). Novel localization of the DNA-PK complex in lipid rafts: a putative role in the signal transduction pathway of the ionizing radiation response. J. Biol. Chem. *278*, 22136–22143.

Matsubara, S., Ding, Q., Miyazaki, Y., Kuwahata, T., Tsukasa, K., and Takao, S. (2013). mTOR plays critical roles in pancreatic cancer stem cells through specific and stemness-related functions. Sci. Rep. *3*, 3230.

McGranahan, N., and Swanton, C. (2017). Clonal heterogeneity and tumor evolution: past, present, and the future. Cell *168*, 613–628.

Mondesire, W.H., Jian, W., Zhang, H., Ensor, J., Hung, M.-C., Mills, G.B., and Meric-Bernstam, F. (2004). Targeting mammalian target of rapamycin synergistically enhances chemotherapy-induced cytotoxicity in breast cancer cells. Clin. Cancer Res. *10*, 7031–7042.

Morales, J.C., Li, L., Fattah, F.J., Dong, Y., Bey, E.A., Patel, M., Gao, J., and Boothman, D.A. (2014). Review of poly (ADP-ribose) polymerase (PARP) mechanisms of action and rationale for targeting in cancer and other diseases. Crit. Rev. Eukaryot. Gene Expr. *24*, 15–28.

Mukherjee, B., Tomimatsu, N., Amancherla, K., Camacho, C.V., Pichamoorthy, N., and Burma, S. (2012). The dual PI3K/mTOR inhibitor NVP-BEZ235 is a potent inhibitor of ATM- and DNA-PKCs-mediated DNA damage responses. Neoplasia *14*, 34–IN38.

Neal, J.A., Xu, Y., Abe, M., Hendrickson, E., and Meek, K. (2016). Restoration of ATM expression in DNA-PKcs-deficient cells inhibits signal end joining. J. Immunol. *196*, 3032–3042.

Nguyen, J.T., Ray, C., Fox, A.L., Mendonça, D.B., Kim, J.K., and Krebsbach, P.H. (2018). Mammalian EAK-7 activates alternative mTOR signaling to regulate cell proliferation and migration. Sci. Adv. *4*, 1–15.

Ostling, O., and Johanson, K.J. (1984). Microelectrophoretic study of radiation-induced DNA damages in individual mammalian cells. Biochem. Biophys. Res. Commun. *123*, 291–298.

Pajonk, F., Vlashi, E., and McBride, W.H. (2010). Radiation resistance of cancer stem cells: the 4 R's of radiobiology revisited. Stem Cells *28*, 639–648.

Pardo, O.E., and Seckl, M.J. (2013). S6K2: the neglected S6 kinase family member. Front. Oncol. *3*, 191.

Pardo, O.E., Wellbrock, C., Khanzada, U.K., Aubert, M., Arozarena, I., Davidson, S., Bowen, F., Parker, P.J., Filonenko, V.V., Gout, I.T., et al. (2006). FGF-2 protects small cell lung cancer cells from apoptosis through a complex involving PKCepsilon, B-Raf and S6K2. EMBO J. *25*, 3078–3088.

Pastrana, E., Silva-Vargas, V., and Doetsch, F. (2011). Eyes wide open: a critical review of sphere-formation as an assay for stem cells. Cell Stem Cell *8*, 486–498.

Peng, D.J., Wang, J., Zhou, J.Y., and Wu, G.S. (2010). Role of the Akt/mTOR survival pathway in cisplatin resistance in ovarian cancer cells. Biochem. Biophys. Res. Commun. *394*, 600–605.

Pérez-Tenorio, G., Karlsson, E., Waltersson, M.A., Olsson, B., Holmlund, B., Nordenskjöld, B., Fornander, T., Skoog, L., and Stål, O. (2011). Clinical potential of the mTOR targets S6K1 and S6K2 in breast cancer. Breast Cancer Res. Treat. *128*, 713–723.

Ploner, C., Kofler, R., and Villunger, A. (2008). Noxa: at the tip of the balance between life and death. Oncogene *27* (*Suppl 1*), S84–S92.

Puck, T.T., and Marcus, P.L. (1956). Action of X-rays on mammalian cells. J. Exp. Med. *103*, 653–666.

Rhodes, D.R., Yu, J., Shanker, K., Deshpandez, N., Varambally, R., Ghosh, D., Barrette, T., Pandeyb, A., and Chinnaiyan, A.M. (2004). ONCOMINE: a cancer microarray database and integrated data-mining platform. Neoplasia *6*, 1–6.

Saxton, R.A., and Sabatini, D.M. (2017). mTOR signaling in growth, metabolism, and disease. Cell *168*, 960–976.

Sharma, K., Vu, T.T., Cook, W., Naseri, M., Zhan, K., Nakajima, W., and Harada, H. (2018). p53-independent Noxa induction by cisplatin is regulated by ATF3/ATF4 in head and neck squamous cell carcinoma cells. Mol. Oncol. *12*, 788–798.

Shibue, T., Takeda, K., Oda, E., Tanaka, H., Murasawa, H., Takaoka, A., Morishita, Y., Akira, S., Taniguchi, T., and Tanaka, N. (2003). Integral role of Noxa in p53-mediated apoptotic response. Genes Dev. *17*, 2233–2238.

Silvera, D., Ernlund, A., Arju, R., Connolly, E., Volta, V., Wang, J., and Schneider, R.J. (2017). mTORC1 and -2 coordinate transcriptional and translational reprogramming in resistance to DNA damage and replicative stress in breast cancer cells. Mol. Cell. Biol. *37*, 1–20.

Smith, G.C.M., and Jackson, S.P. (1999). The DNA-dependent protein kinase. Genes Dev. *13*, 916–934.

Smithson, L.J., and Gutmann, D.H. (2016). Proteomic analysis reveals GIT1 as a novel mTOR complex component critical for mediating astrocyte survival. Genes Dev. *30*, 1383–1388.

Steelman, L.S., Navolanic, P., Chappell, W.H., Abrams, S.L., Wong, E.W., Martelli, A.M., Cocco, L., Stivala, F., Libra, M., Nicoletti, F., et al. (2011). Involvement of Akt and mTOR in chemotherapeutic- and hormonal-based drug resistance and response to radiation in breast cancer cells. Cell Cycle *10*, 3003–3015.

Tu, Y., Ji, C., Yang, B., Yang, Z., Gu, H., Lu, C.-C., Wang, R., Su, Z.-L., Chen, B., Sun, W.-L., et al. (2013). DNA-dependent protein kinase catalytic subunit (DNA-PKcs)-SIN1 association mediates ultraviolet B (UVB)-induced Akt Ser-473 phosphorylation and skin cell survival. Mol. Cancer *12*, 1–12.

Wang, P., Gao, Q., Suo, Z., Munthe, E., Solberg, S., Ma, L., Wang, M., Westerdaal, N.A., Kvalheim, G., and Gaudernack, G. (2013). Identification and characterization of cells with cancer stem cell properties in human primary lung cancer cell lines. PLoS One *8*, e57020.

Weiswald, L.B., Bellet, D., and Dangles-Marie, V. (2015). Spherical cancer models in tumor biology. Neoplasia *17*, 1–15.

Wong, R.H., Chang, I., Hudak, C.S., Hyun, S., Kwan, H.Y., and Sul, H.S. (2009). A role of DNA-PK for the metabolic gene regulation in response to insulin. Cell *136*, 1056–1072.

Wu, C., Jin, X., Tsueng, G., Afrasiabi, C., and Su, A.I. (2016). BioGPS: building your own mash-up of gene annotations and expression profiles. Nucleic Acids Res. *44*, D313–D316.

Wu, C., Macleod, I., and Su, A.I. (2013). BioGPS and MyGene.info: organizing online, gene-centric information. Nucleic Acids Res. *41*, D561–D565.

Wu, C., Orozco, C., Boyer, J., Leglise, M., Goodale, J., Batalov, S., Hodge, C.L., Haase, J., Janes, J., Huss, J.W., 3rd, et al. (2009). BioGPS: an extensible and customizable portal for querying and organizing gene annotation resources. Genome Biol. *10*, R130.

Xie, X., Hu, H., Tong, X., Li, L., Liu, X., Chen, M., Yuan, H., Xie, X., Li, Q., Zhang, Y., et al. (2018). The mTOR-S6K pathway links growth signalling to DNA damage response by targeting RNF168. Nat. Cell Biol. *20*, 320–331.

Zhou, X., Liu, W., Hu, X., Dorrance, A., Garzon, R., Houghton, P.J., and Shen, C. (2017). Regulation of CHK1 by mTOR contributes to the evasion of DNA damage barrier of cancer cells. Sci. Rep. *7*, 1535.

Zhu, Z., Pang, B., Iglesias-Bartolome, R., Wu, X., Hu, L., Zhang, C., Wang, J., Gutkind, J.S., and Wang, S. (2016). Prevention of irradiation-induced salivary hypofunction by rapamycin in swine parotid glands. Oncotarget *7*, 20271–20281.

ISCI, Volume *17*

Supplemental Information

mEAK-7 Forms an Alternative mTOR Complex with DNA-PKcs in Human Cancer

Joe Truong Nguyen, Fatima Sarah Haidar, Alexandra Lucienne Fox, Connor Ray, Daniela Baccelli Mendonça, Jin Koo Kim, and Paul H. Krebsbach

SUPPLEMENTAL INFORMATION

- Transparent Methods
- Figure S1, related to Figure 1: *MEAK7* expression patterns in normal human tissues and cancer patients.
- Figure S2, related to Figure 2 and Figure 3: Normal lymph tissue analysis, H1975 cancer stem cell analysis, and differential cell density clongenicity assay.
- Figure S3, related to Figure 3 and Figure 4: Colony formation assay with second mEAK-7 siRNA, spheroid formation assay with differential cell density or second mEAK-7 siRNA, and mEAK-7 effect of Noxa expression by X-ray irradiation in H1299 cells.
- Figure S4, related to Figure 5 and Figure 6: DNA damage mediated S6K1/2 signaling, and DNA-PKcs binding to S6K1, and second mEAK-7 siRNA effect on DNA damage or nutrient induced S6K2 activation
- Figure S5, related to Figure 6: MDA-MB-231 cell data on mEAK-7 and X-ray irradiation-mediated mTOR signaling.
- Figure S6, related to Figure 6: Dose-dependent analysis of NU7441 on IR-mediated mTOR signaling and DNA-PKcs, mTOR, and PI3K inhibitor study after X-ray irradiation.
- Table S1, related to Figure 5: Immunuoprecipitation-mass spectrometry analysis of mEAK-7.
- Table S2, related to Figure 2: Detailed patient information from US Biomax Tissue Microarrays.

TRANSPARENT METHODS

Cell lines

H1299 and H1975 are non-small cell lung carcinoma cell lines obtained from ATCC. MDA-MB-231 is a triple negative breast carcinoma cell line obtained from ATCC. DNA-PKcs^{WT} and DNA-PKcs$^{-/-}$ HEK-293T cells were kindly gifted from Dr. Kathryn Meek, a Professor at Michigan State University. H1299 cells (ATCC® CRL-5803™) were derived from a 43 year old male, Caucasian. H1975 cells (ATCC® CRL-5908™) were derived from an unknown aged, female. MDA-MB-231 (ATCC® HTB-26™) cells were derived from a 51 year old female Caucasian. HEK-293T cells (ATCC® ACS-4500™) were derived from an unknown aged, human embryonic kidney tissue. All cell lines are of human origin.

Statement of regulatory oversight and approval

The University of Michigan Institutional Review Boards is the committee approving the cell line experiments, approving the use of human samples from US Biomax, and confirming that all experiments conform to the relevant regulatory standards. It is not clear to what extent that sex, gender, and age affected data presented in human tissue microarrays obtained from US Biomax. The influence or association between these characteristics would require further assessment, with regards to the conclusions of this manuscript. Detailed information regarding patient samples from US Biomax can be accessed in Table S2.

Cell culture

Cell culture: Cell lines were grown in Dulbecco's minimal essential medium (DMEM, Thermo Fisher Scientific (TFS): cat# 11995-073), without antibiotics/antimycotics and supplemented with a concentration of 10% fetal bovine serum (FBS, TFS: cat# 10437-036, Lot # 1399413) at 37°C in 5.0% CO_2 incubator. Cells were grown in Falcon™ Tissue Culture Treated Flasks T-75 (Fisher Scientific (FS): cat# 13-680-65) until 75% confluent and split with Trypsin-EDTA 0.25% (TFS: cat# 25200-056) for 5 min in the 37°C cell incubator. Cells were washed 1x with PBS and resuspended in 10% FBS containing DMEM. Cells were counted with the LUNA™ Automated Cell Counter (Logos Biosystems (LB): cat# L10001) utilizing LUNA™ Cell Counting Slides (LB: cat# L12003) and AO-PI dye (LB: cat# F23001).

Small interfering RNA or plasmid transfection

Cells were seeded at a density of 500,000 cells per 60 mm TCP and grown for 24 hours. For siRNA transfection, Lipofectamine® RNAiMAX Transfection Reagent (TFS: cat# 13778-150) was incubated with Opti-MEM® I Reduced Serum Medium (TFS: cat# 31985-070) and 100 nM siRNA was incorporated before introduction to cells at 100 nM concentration. For plasmid transfection, FuGENE® 6 Transfection Reagent (Promega: cat# E2691) was incubated with Opti-MEM I Reduced Serum Medium and 2 µg plasmids were incorporated before introduction into cells. For dual transfection, we added both solutions. siRNAs used were as follows: mEAK-7 #1 siRNA (TFS: ID# s33640). mEAK-7 #2 siRNA (TFS: ID# HSS126697). S6K1 #1 siRNA (TFS: ID#

s12282). S6K1 #2 siRNA (TFS: ID# s12283). S6K2 #1 siRNA (TFS: ID # s12287). S6K2 #2 siRNA (TFS: ID # s12286). Control siRNA (TFS: cat# 4390843). Plasmids were purchased from Addgene. HA-S6K2 plasmid: pcDNA3-S6K2-WT was a gift from John Blenis (Addgene plasmid # 17729).

X-ray irradiation protocol

After appropriate treatment of cells with siRNA, plasmids, chemical compounds, nutrients, etc, we subjected the cells to X-ray irradiation. The machine is a Polaris IC-320 SC-500 series 2 from Kimtron. The dose rate is set at 4.5223Gy/min. X-ray irradiation of cells was done via the 1.5mm Aluminum filter, with a cone which has a 20x20cm beam pattern and a 50 cm FSD (radiation distance). X-ray irradiation applied is either 10 gy or 20 gy.

Immunofluorescence

Deparaffinization and rehydration steps were as follows: xylene for 10 minutes, 100% ethanol for 5 minutes, 95% ethanol for 5 minutes, 70% ethanol for 5 minutes, Milli Q water for 10 minutes, and 1x PBST for 10 minutes. Antigen retrieval steps were as follows: slides were placed in the slide holder to pressure cooker immersed in 10 mM citric acid (pH 6.0). Then, slides were placed in the microwave and cooked at full power for 12.5 minutes, finishing when pressure valve has been up for 1 min. Pressurized steam was exhausted from the pressure cooker. The pressure cooker and slides were cooled under running water for 15 minutes. Slides were washed with 1x PBS for 10

minutes. Slides were permeabilized for 10 minutes with 1x PBS with 0.4%Triton-X. Slides were blocked with 2.5% bovine serum albumin and 1% Tween20 in 1x TBS. Slides were incubated overnight at 4˚C with primary antibody. Next, slides were washed with PBS and incubated in secondary antibodies for 1 hour at room temperature. Slides were washed with PBS with DAPI for 10 minutes. Prolong Gold Antifade with DAPI was used to mount slides (Fisher cat# P36935). Nikon Ti Eclipse Confocal Microscope (60x with oil magnification) was used to capture images. Images were captured with or without 3x digital zoom, 1/32 frames per second, 1024x1024 image capture, 1.2 Airy Units, 2x line averaging, appropriate voltage and power settings optimized per antibody. No image modification was performed, except image sizing reduction for figure preparation. Quantitative analyses were completed via Nikon Analysis Software, with the data analysis and images representing the average of 3 fields of view and more than 50% of the tissue core. NSCLC tissue microarray used for protein level detection of mEAK-7 and p-S6 was purchased from US Biomax (cat# HLug-Squ090Lym-01). Healthy lymph tissue microarray used for protein level detection of mEAK-7 and p-S6 was purchased from US Biomax (cat# LN802A). NSCLC tissue microarray used for patient survival was purchased from US Biomax (cat# HLug-Squ150Sur-02). Primary antibodies for immunofluorescence were as follows: mEAK-7 (Santa Cruz Biotechnology (SCB) cat# sc-247321) and ($Ser^{240/244}$) p-S6 ribosomal protein (D68F8) XP® (Cell Signaling Technologies (CST): cat#5364S). All antibodies were used at 1:1,000 with a working volume of 1.5 mL in 5% BSA in PBS, unless noted otherwise. Secondary antibodies for immunofluorescence were as follows: Donkey anti-Goat IgG

Alexa Fluor® 647 (TFS: cat# A-21447), Anti-rabbit IgG (H+L), and F(ab')2 Fragment Alexa Fluor® 488 Conjugate (CST: cat# 4412S). All antibodies were used at a concentration of 1:1,000, with a working volume of 1.5 mL in 5% BSA in PBS. DAPI stain was used for DNA staining.

Immunoblot analysis

Cells were lysed in cold NP40 lysis buffer (50 mM Tris, 150 mM NaCl, and 1.0% NP-40 at pH 8.0). 50 µg of protein lysate was separated with Novex® Tris-Glycine SDS Running Buffer 10X (TFS: cat# LC2675-4) and Novex™ WedgeWell™ 4-20% Tris-Glycine Gels (TFS; cat# XP04205BOX), NuPAGE™ 3-8% Tris-Acetate Protein Gels (TFS; cat# EA03785BOX). Proteins were transferred to PVDF membranes. 4-20% gels were used for proteins 100 kDa and below, while 3-8% gels were used for proteins 100 kDa and above. Primary antibodies were incubated with membranes overnight at 4°C, and secondary antibodies were incubated with membranes at room temperature for 1 hour. Membranes were incubated with SuperSignal™ West Pico Chemiluminescent Substrate (TFS; cat# 34078) or Femto (TFS; cat# 34095) for film capture on HyBlot CL autoradiography film (Denville Scientific: cat# e3018). Primary antibodies were as follows: α-mEAK-7 (KIAA1609) mouse monoclonal antibody clone OTI12B1 (formerly 12B1) was obtained from Origene Technologies (OT; cat# TA501037, lot A01). All antibodies from Cell Signaling Technologies (CST) are rabbit: α-glyceraldehyde-3-phosphate dehydrogenase (CST: cat# 2118S), α-tubulin (CST: cat# 2144S), α-phospho-S6 ribosomal protein ($Ser^{240/244}$) (CST: cat# 2215S), α-phospho-S6 ribosomal

protein (Ser$^{235/236}$) (CST: cat# 2211S), α-S6 ribosomal protein (CST: cat# 2217S), α-phospho-p70 S6 kinase (Thr^{389}) (CST: cat# 9234S), α-S6K1 (CST: cat# 2708S), α-S6K2 (CST: cat# 14130S), α-mTOR (CST: cat# 2983S), α-HA-tag mouse (CST: cat# 2367S), α-HA-tag rabbit (CST: cat# 3724S), α-(Ser^{65}) p-4E-BP1 (CST: cat# 9451S), α-(Thr$^{37/46}$) p-4E-BP1 (CST: cat# 9459S), α-(Thr^{70}) p-4E-BP1 (CST: cat# 13396S), α-4E-BP1 (CST: cat# 9452S), α-N-cadherin (CST: cat# 13116S), α-noxa (CST: cat# 14766S), α-Cleaved PARP (CST: 5625S), α-(Thr^{68}) p-Chk2 (CST: cat# 2197S), α-Chk2 (CST: cat# 3440S), α-(Ser^{2448}) p-mTOR (CST: cat# 2971S). Concentration of antibodies: p-S6, S6, and 4E-BP1 used at 1:3,000 dilution and remainder at 1:1,000 dilution in 5% BSA in 1X TBST buffer with 0.04% sodium azide. Secondary antibodies for immunoblot analysis: 1:4,000 dilution for α-mouse IgG (Promega; cat# W4021). 1:7,500 dilution for α-rabbit (Promega; cat# W4011), and 1:2,000 dilution for α-rabbit light chain specific antibody (Abcam: cat# ab99697) only for S6K2 IP experiments.

Chemical Inhibitors

All chemical were resuspended in DMSO, according to manufacturer recommendations. Rapamycin (CST; cat# 9904S), LY293002 (CST; cat# 9901S), NU7441 (Tocris Biotechne; cat# 3712). All inhibitors were applied to cells for at least 2 hours, unless stated otherwise in the manuscript.

Immunoprecipitation (IP) analysis and mass spectrometry

After siRNA and/or plasmid transfection, cells were harvested in 1% NP40 lysis buffer or CHAPS lysis buffer (FIVEphoton Biochemicals (FB): cat# CIB-1) supplemented with protease inhibitors (FB: cat# PI-1) and phosphatase inhibitors (FB: cat# PIC1). For antibody-bead conjugation, 1 to 2 µg of antibodies and 50 µL of mixed Protein A/G PLUS-Agarose (SCB; Cat # sc-2003) were incubated for 1 hour on vertical shaker at 4°C. Afterwards, the antibody-bead mix was washed 3 times with 1x PBS. Next, 250 µg of protein in CHAPS buffer were incubated with the antibody-bead mix for 1.5 hours on vertical shaker at 4°C. After incubation, the antibody-bead conjugates were washed 3 times with 1x PBS. Beads were washed 3 times with 1x PBS, and 3x loading buffer with SDS was added to the bead mix, boiled, spun down, and utilized for immunoblot analysis. Immunoprecipitation-mass spectrometry: Samples were processed by the University of Michigan Proteomics core for IP/MS analysis and protocols can be found on their webpage. Samples submitted to the core were pooled from 3x reactions of HA-mEAK-7 in H1299 cells, as described above. Full excel sheet supplied as Table S1. Antibodies used for immunoprecipitation reactions were as follows: Anti-HA epitope tag polyclonal goat IgG Antibody (Novus Biologicals: cat# NB600-362), polyclonal goat IgG antibody (SCB: cat# sc-2028), α-S6K2 (CST: cat# 14130S), α-mTOR (CST: cat# 2983S), mEAK-7 (SCB, cat# sc-247321).

Cell Invasion assay

After siRNA transfection and X-ray irradiation, cells were trypsinized and 50,000 cells were seeded onto Corning® Matrigel® Invasion Chamber 24-Well Plate 8.0 Micron

(Corning: cat# 354480), with 1 mL of DMEM^{-AAs} without FBS within the top chamber, and 1 mL of 10% FBS-containing DMEM medium on the bottom of the plate. After 24 hours, we processed the samples with Hema 3™Stat Pack (Fisher: cat# 123-869), according to manufacturer specifications. Images were captured with a stereoscope, attached to a digital camera. Brightness and contrast were adjusted, as needed. Analysis was conducted via student's t-test. % invasion was counted on 6 individual experiments per condition as: # cells adhered to the bottom chamber divided by # cells seeded total.

Comet Assay

Lysis Buffer, Alkaline Solution, and Eletrophoresis Running Solution were prepared according to manufacturer's instructions. Solutions were stored at 4°C. Oxiselect Comet Agarose (Cell Bio Labs (CBL): #235002) was heated to 95°C for 20 minutes, then placed in 37°C water bath until use. Cells were grown according to experimental procedures for siRNA treatment. Two days post siRNA treatment, cells were subjected to no treatment, 2 gy, and 6 gy X-ray irradiation. Cells were trypsinized and resuspended at a concentration of $1x10^5$ cells/mL in cold PBS. Then, 10 µL of cell suspension was mixed with 90 µL of comet agarose. After mixing thoroughly, 75 µL of this mixture was transferred to the OxiSelect Comet Slide (CBL: #STA-352). Slides were placed in the dark at 4°C for 15 minutes. Slides were transferred to a small basin containing pre-chilled Lysis buffer and placed at 4°C for 60 minutes in the dark. Lysis solution was aspirated from the basin, replaced with pre-chilled Alkaline solution, and

placed at 4°C in the dark for 30 minutes. Then, Alkaline solution was aspirated and replaced with pre-chilled TBE Electrophoresis solution. After 5 minutes, TBE Electrophoresis solution was aspirated and replaced with new TBE Electrophoresis solution. Slides were transferred to a horizontal electrophoresis chamber and the well was filled with enough TBE Electrophoresis solution to fully cover the slides. Voltage was applied for 45 minutes at 20 volts. After electrophoresis, slides were transferred to a small basin containing pre-chilled DI H2O, and the slides were fully immersed. After 2 minutes, the DI H2O was aspirated and replaced. This rinse was repeated twice. After the third rinse, slides were immersed in cold 70% ethanol for 5 minutes, then removed from the basin and allowed to air dry. Once the agarose was dried fully, 100 µL of diluted Vista Green DNA dye (CBL: cat# 235003, diluted 1:10,000 in TE buffer) was added to each well and allowed to incubate at room temperature for 15 minutes. Slides were imaged with Nikon Ti Eclipse Confocal Microscope at 10x magnification lens to capture images. Images were captured at 1/8 frames per second, 1024x1024 image capture, 1.2 Airy Units, 2x line averaging, appropriate voltage and power settings for FITC (488 nm). No image modification was performed, except image sizing reduction for figure preparation.

Cancer Stem Cell sorting

Cells were trypsinized and resuspended in DMEM medium with 10% FBS and counted on Luna cell counter (Logos Biosystems (LB): cat# L10001) using Acridine Orange/Propidium Iodide dye (LB: cat# F23001) for viability. $1x10^7$ cells were filtered

into each of 5 labeled 50 mL falcon tubes, through a 40 µm filter. $1x10^7$ cells were filtered into each of 5 labeled 5 mL round bottom tubes (Falcon: cat# 352235) to be used as single-color controls. Tubes were centrifuged at 1,000 rpm for 4 minutes at 4°C and supernatant was discarded. One 5 mL single color control tube was resuspended with 200 μL PBS with 10% FBS to be used as a negative control. Three of the other single-color control tubes were resuspended with 200 µL PBS with 10% FBS, and single color dyes were added as detailed: 2 µL DAPI (Thermo Fisher: cat# D1306), 25 µL CD90 (Biolegend: cat# 328107), and 10 µL CD44 (BD Biosciences: cat# 559942). The final single-color tube was used for Isotype control. This pellet was resuspended with 191 µL PBS with 10% FBS and 2 µL DAPI, 2 µL APC Isotype (BD Biosciences: cat# 340442), and 5 µL FITC Isotype (BD Bioscience: cat# 555909) were added. Cells in the 50 mL tubes were resuspended with 10 mL PBS with 10% FBS. The stain master mix was added to each tube to be sorted. Tubes were placed on a rack and incubated at 37°C for 30 minutes. Cells were rinsed with 1x PBS and resuspended 1x PBS containing 3% FBS. Place all tubes on ice until samples will be run on Flow Cytometer (Sony: Cat# SH800).

Clonogenicity Assay

Cells were grown according to experimental procedures for siRNA treatment. Two days post siRNA treatment, cells were subjected to no treatment, 2 gy, and 6 gy X-ray irradiation. 10,000 H1975 cells or 2,500 H1299 cells were plated into 60 mm dishes with 2 mL DMEM with 10% FBS. Cells were cultured in the incubator for 10 days (until

control colonies contained >50 cells), and new media and new siRNA were added every 4 days. Cells were fixed with 2 mL of fixation mix (glacial acetic acid (Sigma-Aldrich 537020) and methanol (Sigma-Aldrich 67-56-1), at a 1:7 ratio) for 2-3 minutes at room temperature and incubated with 2 mL Crystal Violet (Sigma-Aldrich C6158-50G, diluted to 0.5% in Milli-Q water) for 2 hours at room temperature. After 2 hours, the Crystal Violet was removed and the dishes were rinsed with 2 mL of media (no FBS added), pipetting vigorously to dislodge cells. Dishes were rinsed carefully in DI water and placed on paper towel to dry for 2-3 days. Once plates were dry, colonies were counted and recorded.

Spheroid Formation Assay

Cells were grown according to normal experimental procedures for siRNA treatment (n=6). Two days post siRNA treatment, cells were subjected to no treatment, 2 gy and 6 gy X-ray irradiation. 10,000 H1975 cells or 5,000 H1299 cells were plated into ultralow attachment plates (Costar: cat# 3471). 2 mL of Serum Free Medium (435 mL MEBM Medium (Lonza: cat# CC-3151), 10 mL B27 (Gibco: cat# 17504-044), 5 mL Pen/Strep (Gibco: cat# 15070), 5 mL Lipid Concentrate (Gibco: cat# 11905-031), 2.5 mL Insulin (Sigma-Aldrich: cat# I6634), 10 µg EGF (BD Biosciences: cat# 354052), 10 µg bFGF (BD Bioscience: cat# 354060), 500 µg Hydrocortisone (Sigma-Aldrich: cat# H4001), 500 µL 100 mM ß-mercaptoethanol (Sigma-Aldrich: cat# M3148), 2 mg Cholesterol (Sigma-Aldrich: cat# C4951)) were added to each well. Cells were grown for 2 weeks, adding 500 µL of Serum Free Medium every 4 days to ensure cells have adequate nutrients.

After 2 weeks, the number of spheres growing in each well (spheres must have defined, circular edges and be made of at least 10 cells) was counted, and representative images of spheres from each treatment group were taken.

Statistical analysis and reproducibility

GTEx data acquisition, processing, and statistical analysis information can be found on "gtexportal.org". cBioportal was accessed by searching for "*MEAK7*" or "*MEAK7*: gain amp". Patient derived data from Oncomine were analyzed via unpaired student's t-test. Patient derived tissue microarray data were analyzed via paired Mann-Whitney's U-test. 2D/3D clonogenicity assay, comet assay, cell proliferation, cell migration, and cell size were analyzed via paired student's t-test. Immunoblot and immunoprecipitation assays were repeated at least thrice in all cell lines.

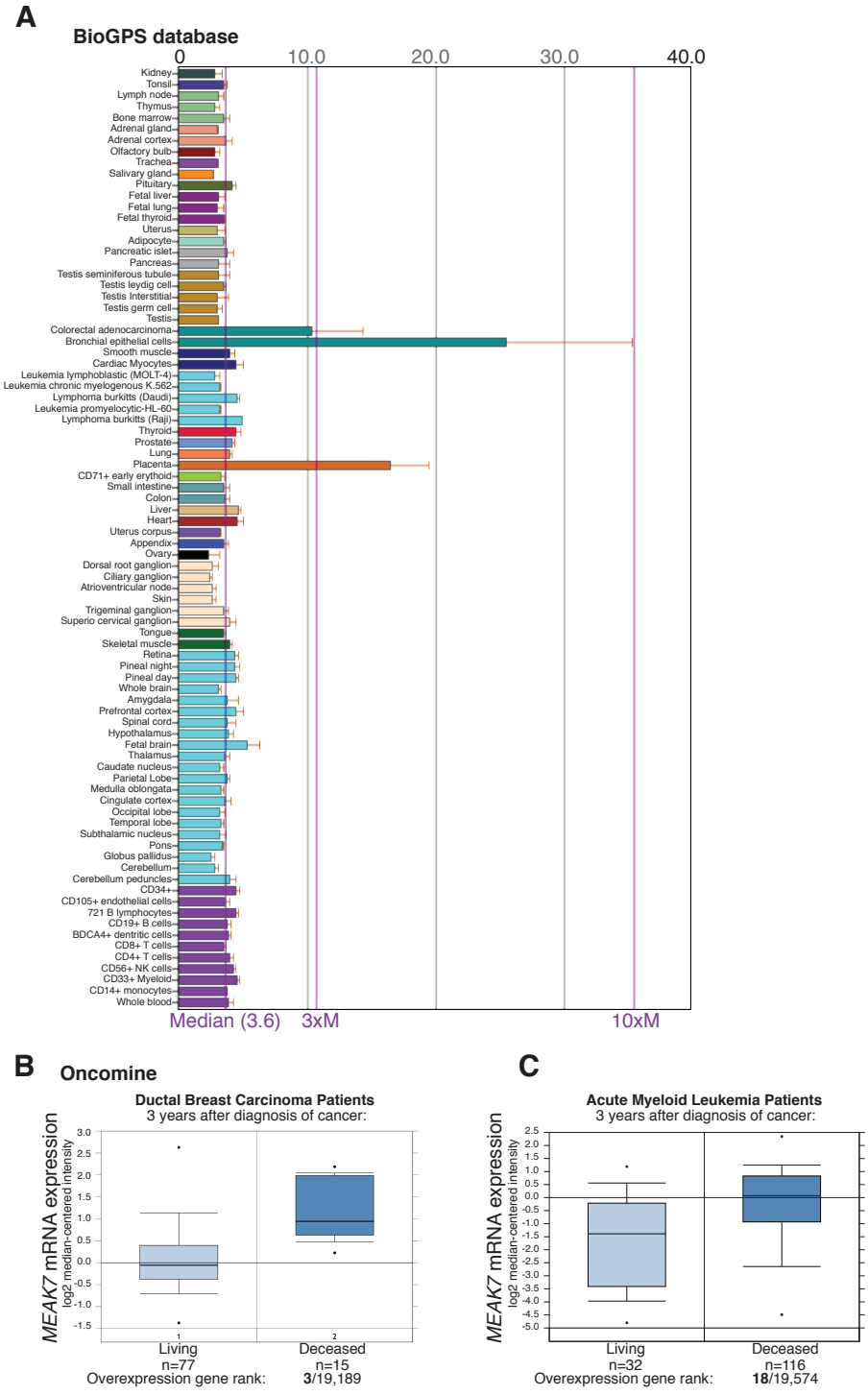
A
BioGPS database
0
10.0
20.0
30.0
40.0
Kidney
Tonsil
Lymph node
Thymus
Bone marrow
Adrenal gland
Adrenal cortex
Olfactory bulb
Trachea
Salivary gland
Pituitary
Fetal liver
Fetal lung
Fetal thyroid
Uterus
Adipocyte
Pancreatic islet
Pancreas
Testis seminiferous tubule
Testis leydig cell
Testis Interstitial
Testis germ cell
Testis
Colorectal adenocarcinoma
Bronchial epithelial cells
Smooth muscle
Cardiac Myocytes
Leukemia lymphoblastic (MOLT-4)
Leukemia chronic myelogenous K-562
Lymphoma burkitts (Daudi)
Leukemia promyelocytic-HL-60
Lymphoma burkitts (Raji)
Thyroid
Prostate
Lung
Placenta
CD71+ early erythroid
Small intestine
Colon
Liver
Heart
Uterus corpus
Appendix
Ovary
Dorsal root ganglion
Ciliary ganglion
Atrioventricular node
Skin
Trigeminal ganglion
Superio cervical ganglion
Tongue
Skeletal muscle
Retina
Pineal night
Pineal day
Whole brain
Amygdala
Prefrontal cortex
Spinal cord
Hypothalamus
Fetal brain
Thalamus
Caudate nucleus
Parietal Lobe
Medulla oblongata
Cingulate cortex
Occipital lobe
Temporal lobe
Subthalamic nucleus
Pons
Globus pallidus
Cerebellum
Cerebellum peduncles
CD34+
CD105+ endothelial cells
721 B lymphocytes
CD19+ B cells
BDCA4+ dentritic cells
CD8+ T cells
CD4+ T cells
CD56+ NK cells
CD33+ Myeloid
CD14+ monocytes
Whole blood
Median (3.6)
3xM
10xM
B
Oncomine
Ductal Breast Carcinoma Patients
3 years after diagnosis of cancer:
MEAK7 mRNA expression
log2 median-centered intensity
Living
n=77
Deceased
n=15
Overexpression gene rank:
3/19,189
C
Acute Myeloid Leukemia Patients
3 years after diagnosis of cancer:
MEAK7 mRNA expression
log2 median-centered intensity
Living
n=32
Deceased
n=116
Overexpression gene rank:
18/19,574

287

Figure S1, related to Figure 1. *MEAK7* is expressed at basal levels in many normal human tissues, but significantly overexpressed in human cancer patients with mortality. (**A**) BioGPS analysis of *MEAK7* in human tissues and cells. (**B, C**) Oncomine analysis of *MEAK7* gene expression of patients with (b) ductal breast carcinoma (P=2.72x10^{-6}, Fold Change: 2.136) and (c) acute myeloid leukemia (P=7.99x10^{-6}, Fold Change: 2.655).

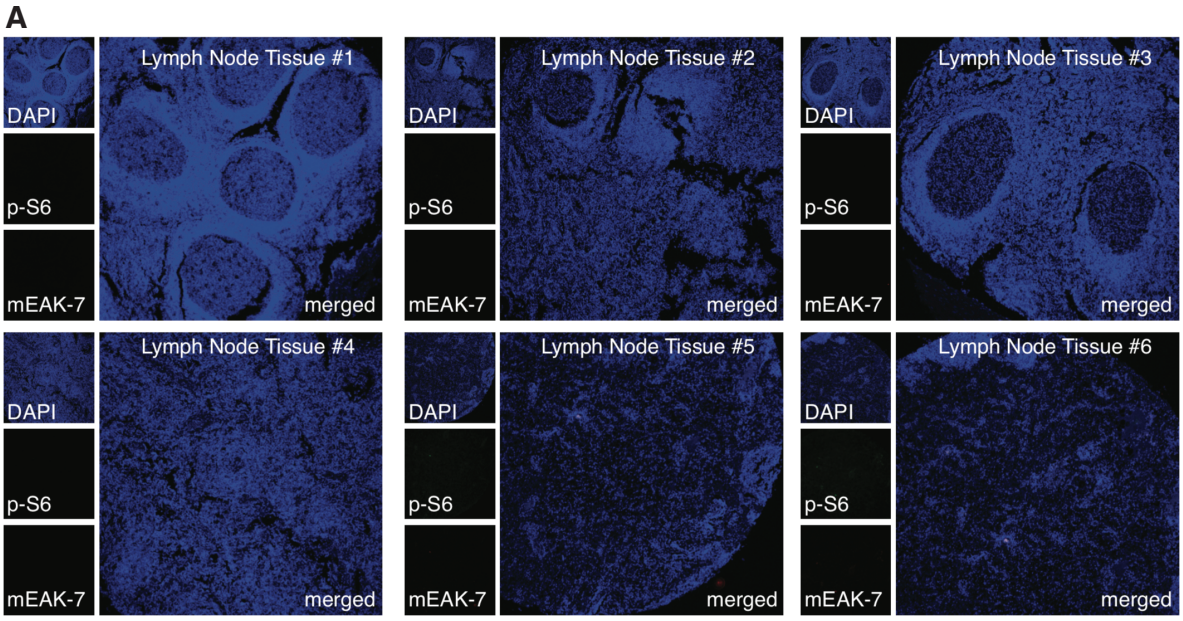
A
Lymph Node Tissue #1
Lymph Node Tissue #2
Lymph Node Tissue #3
Lymph Node Tissue #4
Lymph Node Tissue #5
Lymph Node Tissue #6
DAPI
p-S6
mEAK-7
merged

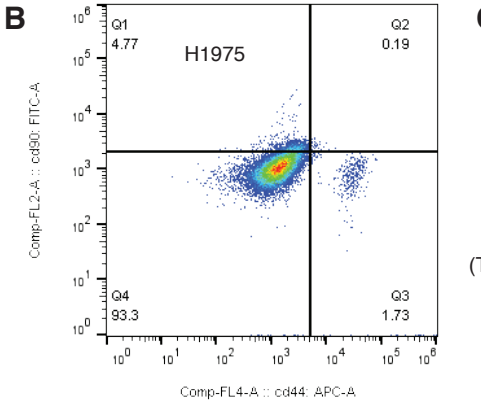
B
H1975
Q1
4.77
Q2
0.19
Q4
93.3
Q3
1.73
Comp-FL2-A :: cd90: FITC-A
Comp-FL4-A :: cd44: APC-A

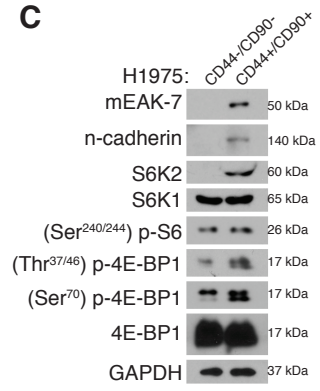
C
H1975:
CD44-/CD90-
CD44+/CD90+
mEAK-7
n-cadherin
S6K2
S6K1
(Ser240/244) p-S6
(Thr37/46) p-4E-BP1
(Ser70) p-4E-BP1
4E-BP1
GAPDH
50 kDa
140 kDa
60 kDa
65 kDa
26 kDa
17 kDa
17 kDa
17 kDa
37 kDa

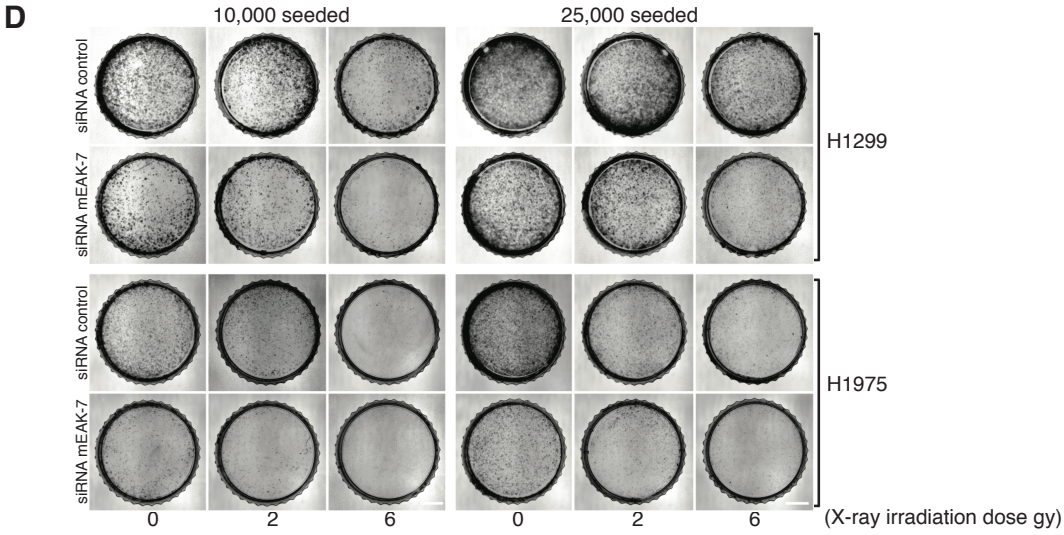
D
10,000 seeded
25,000 seeded
siRNA control
siRNA mEAK-7
H1299
H1975
0
2
6
(X-ray irradiation dose gy)

310

Figure S2, related to Figure 2 and Figure 3. Normal lymph tissue analysis, H1975 cancer stem cell analysis, and differential cell density clongenicity assay. (**A**) 6 representative sections of US Biomax tissue microarray LN802a was analyzed using the antibodies against mEAK-7 and p-S6. (**B**) Flow sort diagram depicting the CD44+/CD90+ cell population in H1975 cells. (**C**) Immunoblot analysis of CD44-/CD90- and CD44+/CD90+ H1975 cells for mEAK-7 and mTOR signaling. (**D**) H1299 and H1975 cells were treated with control or mEAK-7 siRNA, X-irradiated at 2 or 6 gy, and 10,000 or 25,000 cells were seeded into 60 mm TCPs and grown for 10 days. White bars denote 2.5 mm. This experiment was repeated at least 6 times.

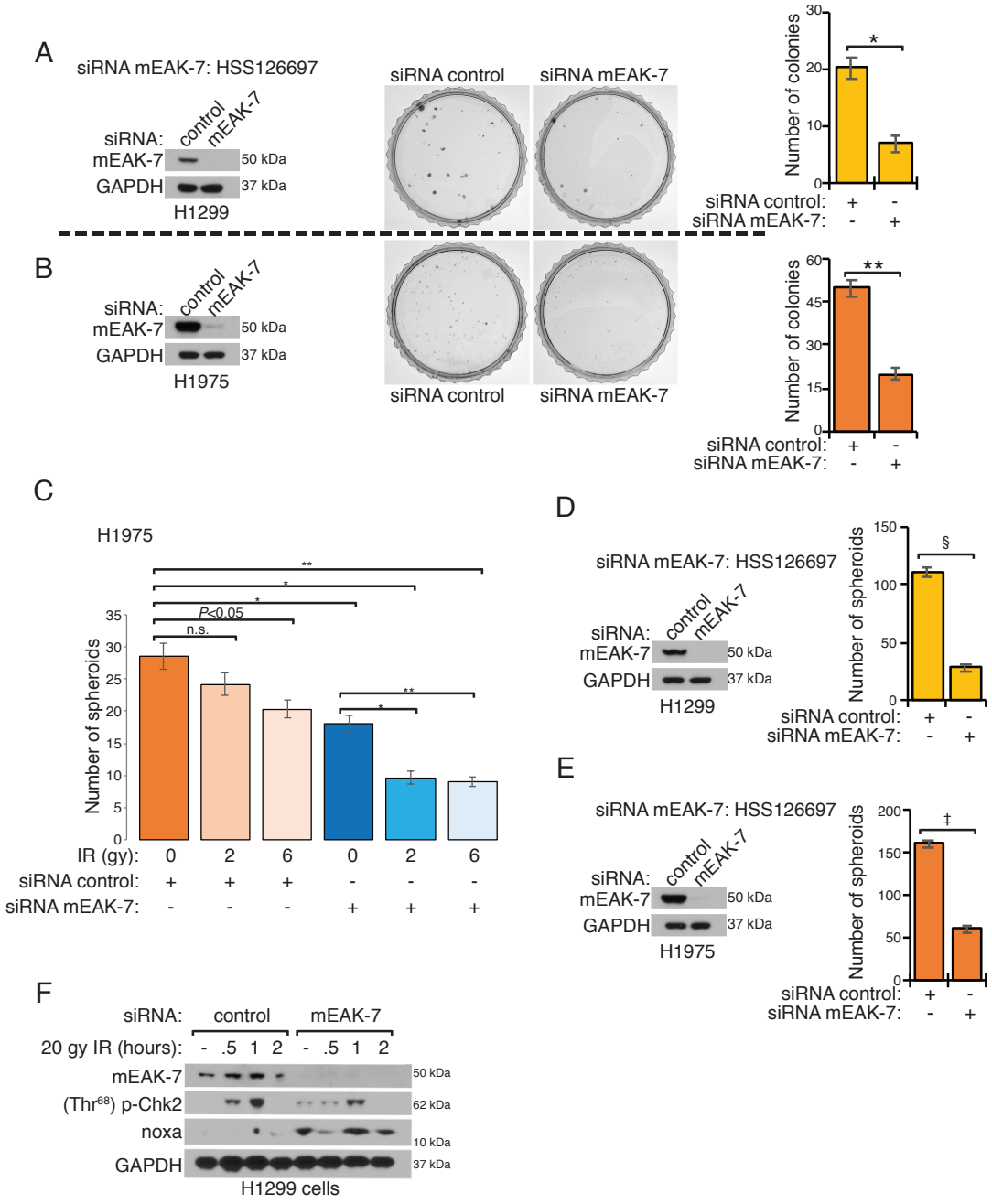

Figure S3, related to Figure 3 and Figure 4. Colony formation assay with second mEAK-7 siRNA, spheroid formation assay with differential cell density or second mEAK-7 siRNA, and mEAK-7 effect of Noxa expression by X-ray irradiation in H1299 cells. (**A**) H1299 cells were treated with control or mEAK-7 siRNA (ID: HSS126697) for 48 hours, and 500 cells were seeded into 60 mm TCPs and grown for

10 days. Quantification of colony formation and analysis via student's t-test (n=6) of (A), *P<0.01. (**B**) H1975 cells were treated with control or mEAK-7 siRNA (ID: HSS126697) for 48 hours, and 500 cells were seeded into 60 mm TCPs and grown for 10 days. Quantification of colony formation and analysis via student's t-test (n=6) of (B), *P<0.01, **P<0.001. (**C**) H1975 cells were treated with control or mEAK-7 siRNA, subjectd to no treatment, 2 gy, or 6 gy of X-ray irradiation, and 5,000 cells were seeded into 60 mm ultra-low attachment plates and grown for 10 days. Quantification of spheroid formation and analysis via student's t-test (n=6), *P<0.01, **P<0.001. (**D**) H1299 cells were treated with control or mEAK-7 siRNA (ID: HSS126697), and 2,500 cells were seeded into 60 mm ultra-low attachment plates and grown for 10 days. Quantification of spheroid formation and analysis via student's t-test (n=6) of (D), *P<0.01, **P<0.001, ***P<0.0001, ‡P<0.00001, §P<0.000001. (**E**) H1975 cells were treated with control or mEAK-7 siRNA (ID: HSS126697), and 5,000 cells were seeded into 60 mm ultra-low attachment plates and grown for 10 days. Quantification of spheroid formation and analysis via student's t-test (n=6) of (E), *P<0.01, **P<0.001, ***P<0.0001, ‡P<0.00001, §P<0.000001. (F) H1299 cells were treated with control or mEAK-7 siRNA and X-ray irradiated at 20 gy for 30 minutes, 1 hour, or 2 hours and analyzed for Noxa expression by DNA damage.

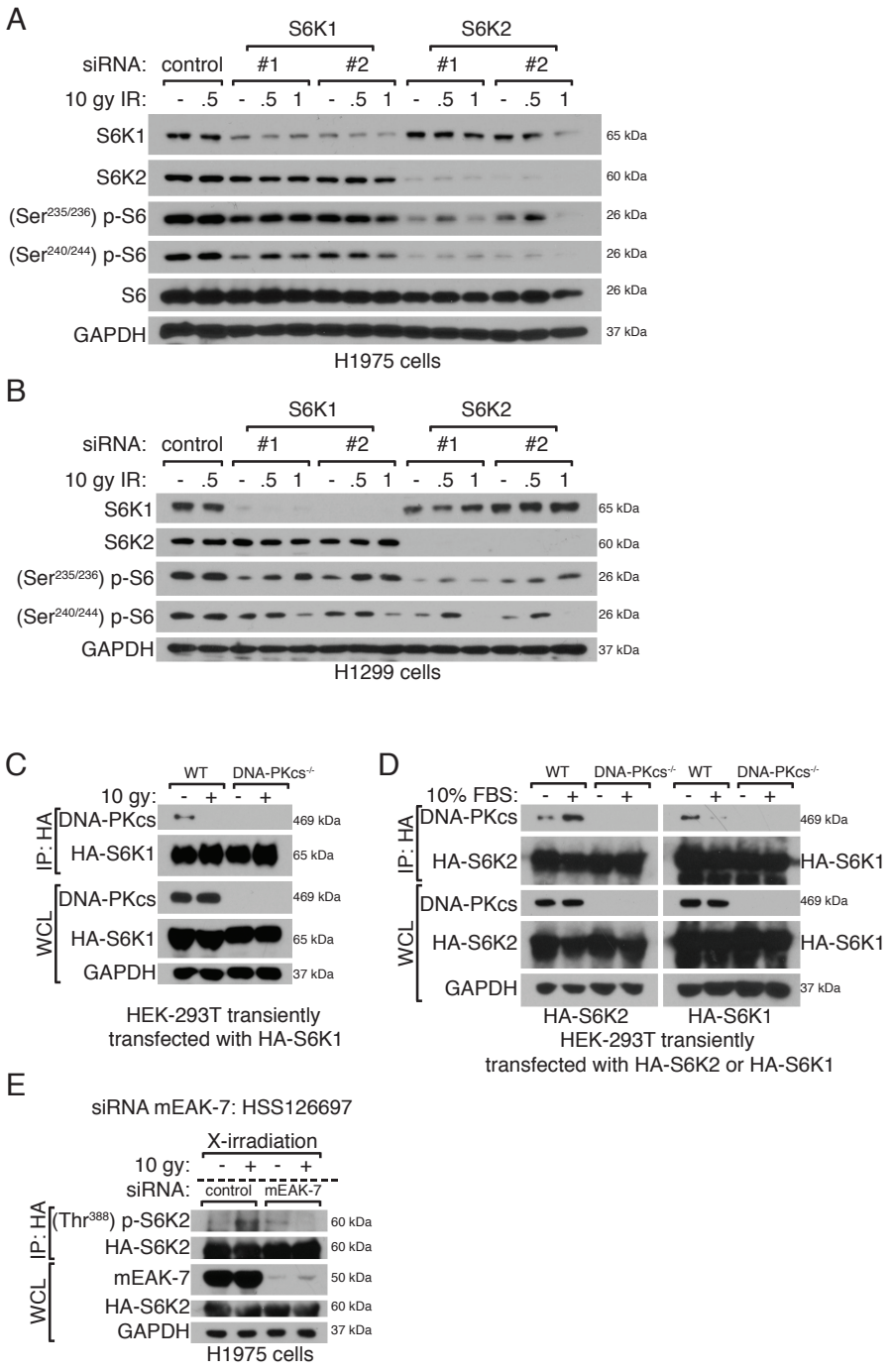

Figure S4, related to Figure 5 and Figure 6. DNA damage mediated S6K1/2 signaling, and DNA-PKcs binding to S6K1, and second mEAK-7 siRNA effect on DNA damage or nutrient induced S6K2 activation. (**A**) H1975 cells were treated with control, 2 unique S6K1, or 2 unique S6K2 siRNAs, then subjected to no treatment, 10

gy of X-ray irradiation for 30 minutes or 1 hour. Immunoblot analysis on mTOR signaling. (**B**) H1299 cells were treated with control, 2 unique S6K1, or 2 unique S6K2 siRNAs, then subjected to no treatment, 10 gy of X-ray irradiation for 30 minutes or 1 hour. Immunoblot analysis on mTOR signaling. (**C**) HEK-293T DNA-PKcs$^{+/+}$ or HEK-293T DNA-PKcs$^{-/-}$ cells were transiently transfected with or without pRK7-HA-S6K1-WT, then untreated or treated with 10 gy of X-ray irradiation for 1 hour. HA-S6K1 was immunoprecipitated to check DNA-PKcs interaction. This experiment was completed at least 3 times. (**D**) HEK-293T DNA-PKcs$^{+/+}$ or HEK-293T DNA-PKcs$^{-/-}$ cells were transiently transfected with pcDNA3-HA-S6K2 or pRK7-HA-S6K1-WT for 48 hurs. Next, cells were starved in DMEM^{-AAs} for 1 hour and reintroduced with 10% FBS in DMEM^{AAs} for 30 minutes. Cells were collected in CHAPS lysis buffer and immunoprecipitated with HA antibody. (**E**) H1975 cells were transiently transfected with pcDNA3-HA-S6K2 and control or mEAK-7 siRNA (ID: HSS126697) for 48 hours. Next, cells were untreated or treated with 10 gy of X-ray irradiation for 30 minutes, followed by IP of HA-S6K2, and probed for activated S6K2 signaling.

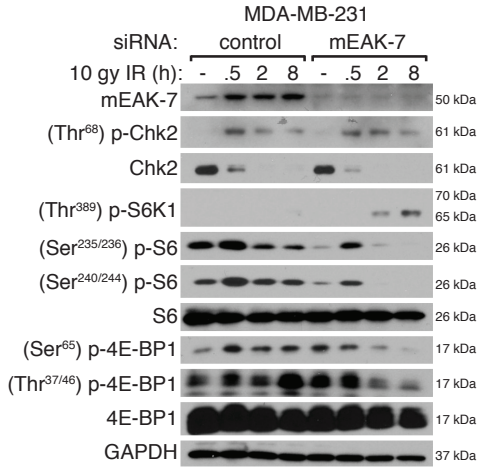

Figure S5, related to Figure 6. mEAK-7 is required for X-ray irradiation-mediated mTOR signaling in MDA-MB-231 cells. MDA-MB-231 cells were treated with control or mEAK-7 siRNA for 48 hours, X-irradiated at 10 gy for 30 minutes, 2 hours, and 8 hours and processed for mTOR signaling. This experiment was completed at least 3 times.

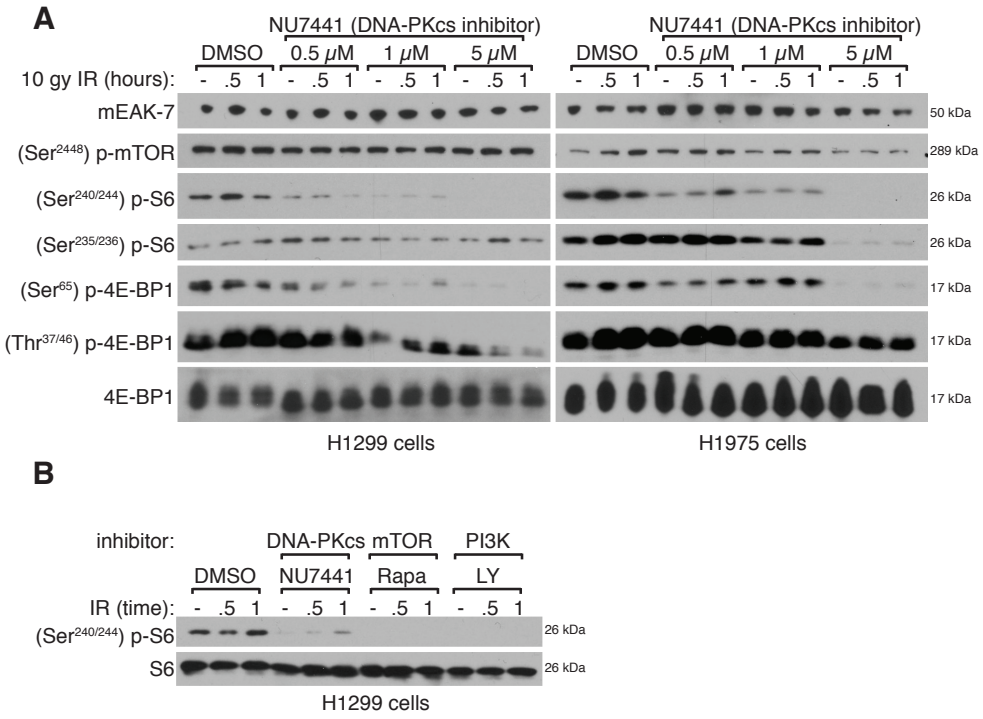

Figure S6, related to Figure 6. Dose-dependent analysis of NU7441 on IR-mediated mTOR signaling and inhibition of DNA-PKcs, mTOR, and PI3K significantly decreased IR-mediated mTOR signaling in H1299 cells. (**A**) H1299 and H1975 cells were treated with DMSO or 0.5 μM, 1 μM, 5 μM NU7441 for 2 hours before treated with X-ray irradiation at 10 gy for 30 minutes and 1 hour. Immunoblot analysis on mTOR signaling. All experiments were repeated at least 3 times. 4E-BP1 was utilized as a loading control. (**B**) H1299 cells were treated with inhibitors of DNA-PKcs (5 μM NU7441, IC50 = 14 nM), mTOR (100 nM rapamycin, IC50 = 1 nM), and PI3K (50 μM LY249002, IC50 = 2.3 μM) for 1 hour before treated with X-ray irradiation at 10 gy for 30 minutes and 1 hour. Immunoblot analysis on mTOR signaling. We observed that inhibition of DNA-PKCS, mTOR, or PI3K significantly decreased IR-

mediated mTOR signaling. All experiments were repeated at least 3 times. S6 was utilized as a loading control.

Table S1. Immunoprecipitation-mass spectrometry analysis of HA-mEAK-7.

Extended full list of proteins from IP-MS experiment for Figure 5A.

Table S2: Detailed patient information from US Biomax TMAs. Detailed patient information regarding TMAs analyzed for Figure 2A-C, Figure 2D, and Figure S2.